HHS Public Access

Author manuscript

Cell Metab. Author manuscript; available in PMC 2023 November 01.

Published in final edited form as:

Cell Metab. 2022 November 01; 34(11): 1749–1764.e7. doi:10.1016/j.cmet.2022.09.008.

Extra-cardiac BCAA catabolism lowers blood pressure and protects from heart failure

Danielle Murashige[1], **Jae Woo Jung**[1], **Michael D. Neinast**[1,2], **Michael G. Levin**[1], **Qingwei Chu**[1], **Jonathan P. Lambert**[3], **Joanne F. Garbincius**[3], **Boa Kim**[1], **Atsushi Hoshino**[1,4], **Ingrid Marti-Pamies**[1], **Kendra McDaid**[1], **Swapnil V. Shewale**[1], **Emily Flam**[1], **Steven Yang**[1,5], **Emilia Roberts**[1], **Li Li**[1], **Michael P. Morley**[1], **Kenneth C. Bedi Jr.**[1], **Matthew C. Hyman**[1], **David S. Frankel**[1], **Kenneth B. Margulies**[1], **Richard K. Assoian**[1], **John W. Elrod**[3], **Cholsoon Jang**[2,6], **Joshua D. Rabinowitz**[2], **Zoltan Arany**[1,#]

[1]Division of Cardiovascular Medicine, Perelman School of Medicine at the University of Pennsylvania, Philadelphia, PA USA 19104.

[2]Ludwig Institute for Cancer Research, Princeton Branch, Princeton, NJ 08544, USA

[3]Cardiovascular Research Center, Lewis Katz School of Medicine at Temple University, Philadelphia, PA, 19140.

[4]Department of Cardiovascular Medicine, Graduate School of Medical Science, Kyoto Prefectural University of Medicine, Kyoto, Japan

[5]Washington University School of Medicine, Washington University in St. Louis, St. Louis, MO, 63110

[6]Department of Biological Chemistry, University of California Irvine, Irvine, CA, 92697.

Summary

Pharmacologic activation of branched chain amino acid (BCAA) catabolism is protective in models of heart failure (HF). How protection occurs remains unclear, although a causative block

[#]Lead Contact: zarany@pennmedicine.upenn.edu.

Author contributions

D.M., M.N., and Z.A. designed the study. D.M. executed most experiments with help from M.N., J.W.J., and S.Y. Mass spectrometry was performed by C.J. and M.N. Mendelian randomization studies were done by M.L. Q.C. performed catheter placement surgery. J.L. performed BT2 study at Temple University. A.H. generated *Bckdk*$^{fl/fl}$ mouse. MI surgeries were performed by the Penn CVI Physiology Core (K.M.); echocardiography was performed by J.F.G. and the Penn CVI Physiology Core (S.V.S. and I.M.P.). B.K. and E.R. performed carotid artery constriction/dilation experiment. L.L. performed histological sectioning and staining. D.F. and M.H. recruited participants and collected arterial and coronary sinus blood samples. E.F., K.B., and K.M. procured and curated human cardiac tissue samples and associated clinical metadata; E.F. analyzed tissue metabolomics; M.P.M. analyzed tissue RNA-Seq. D.M. and Z.A. wrote the manuscript. All authors discussed the results and commented on the manuscript.

Declaration of Interests

Z.A. received consulting fees from Pfizer. J.W.E. received consulting fees, unassociated with this work, from Jannsen Pharmaceuticals and Mitobridge, Inc. J.D.R. is an advisor and stockholder in Colorado Research Partners, Empress Therapeutics, L.E.A.F. Pharmaceuticals, Bantam Pharmaceuticals, Barer Institute, and Rafael Holdings; a founder, director, and stockholder of Farber Partners, Serien Therapeutics, and Sofro Pharmaceuticals; a founder and stockholder in Toran Therapeutics; inventor of patents held by Princeton University; and a director of the Princeton University-PKU Shenzhen collaboration.

in cardiac BCAA oxidation is widely assumed. We use here in vivo isotope infusions to show that cardiac BCAA oxidation in fact increases, rather than decreases, in HF. Moreover, cardiac-specific activation of BCAA oxidation does not protect from HF, even though systemic activation does. Lowering plasma and cardiac BCAAs also fails to confer significant protection, suggesting alternative mechanisms of protection. Surprisingly, activation of BCAA catabolism lowers blood pressure (BP), a known cardioprotective mechanism. BP lowering occurred independently of nitric oxide and reflected vascular resistance to adrenergic constriction. Mendelian randomization studies revealed that elevated plasma BCAAs portend higher BP in humans. Together, these data indicate that BCAA oxidation lowers vascular resistance, perhaps in part explaining cardio-protection in HF that is not mediated directly in cardiomyocytes.

Graphical Abstract

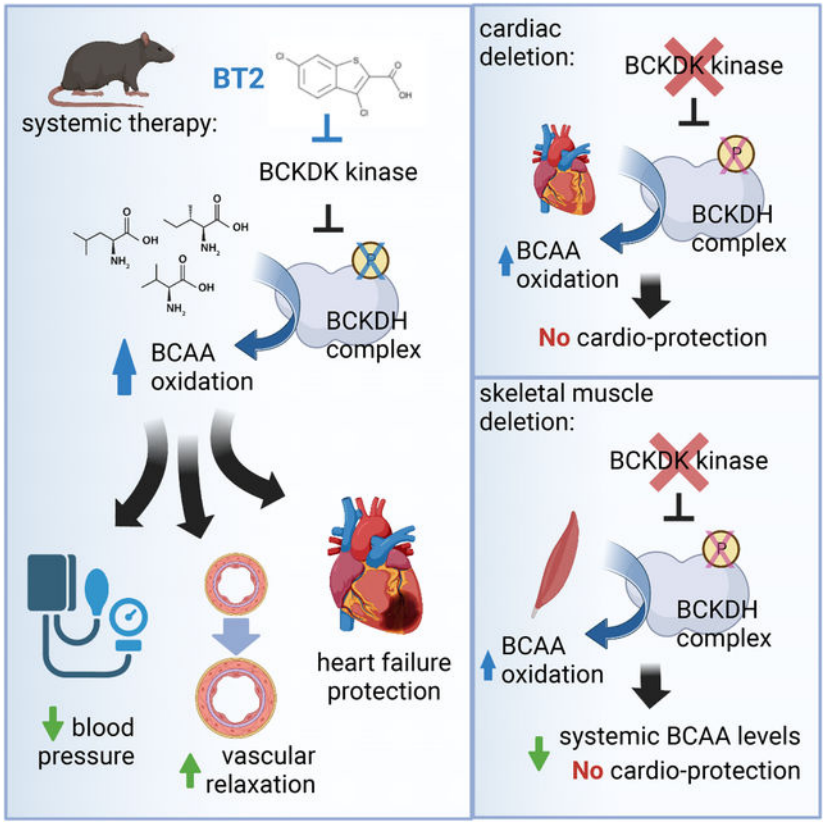

eTOC

Murashige et al. report that the widely studied cardio-protection afforded by pharmacological activation of BCAA oxidation in mice is not mediated by oxidation in cardiomyocytes, nor by lowering BCAA levels. Instead, the authors surprisingly find that enhanced BCAA oxidation lowers blood pressure and promotes vasorelaxation, perhaps explaining the observed cardio-protection.

Introduction

Heart failure (HF) is a leading cause of death worldwide, and the leading cause of hospital admissions in patients over 65 in the US (Virani et al., 2020). Despite major treatment advances made over the past 40 years, the five-year mortality rate for patients with HF remains ~50%. Neurohormonal blockade has been the mainstay of HF management for decades, but the limits of its benefits have likely been reached. Novel therapies, addressing novel pathways, are thus needed.

Mounting evidence suggests that the failing heart is an “engine out of fuel” that fails to use fuel appropriately to satisfy its metabolic demands. In the failing human heart, high-energy phosphate levels are reduced by as much as 40%, via mechanisms still incompletely understood (Ingwall and Weiss, 2004; Neubauer, 2007). Most research in cardiac metabolism has to date focused on glucose, fatty acid, and lactate as fuels, but there is now increasing evidence for altered metabolism of amino acids and ketones. Among the most striking recent findings is an elevation of circulating plasma branched chain amino acids (BCAAs: leucine, isoleucine, and valine) in patients with coronary artery disease (CAD) (Bhattacharya et al., 2014; McGarrah et al., 2018; Shah et al., 2010, 2012), which is associated with subsequent adverse events (Du et al., 2018b, 2018a). The expression of BCAA catabolic genes is suppressed in failing human heart and is the most significantly suppressed metabolic pathway in failing murine heart (Sun et al., 2016). In numerous mouse models, whole-body genetic suppression of BCAA catabolism worsens HF(Li et al., 2017; Sun et al., 2016), and dietary BCAA supplementation worsens contractility and increases infarct size following myocardial infarction (Wang et al., 2016). Conversely, systemic pharmacological activation of BCAA catabolism attenuates HF in mice subjected to transverse aortic banding, ischemia/reperfusion, and myocardial infarction (Li et al., 2017; Sun et al., 2016; Wang et al., 2016). These data compellingly indicate that activating BCAA catabolism can profoundly benefit HF.

What remains unclear, however, is the mechanism by which lowering BCAAs benefits HF. The simplest explanation, generally assumed, is that cardiac oxidation of BCAAs is beneficial, and is inappropriately suppressed in HF. Proposed mechanisms by which suppressed BCAA catabolism might promote HF include loss of fuel contribution to ATP generation, cross-inhibition of carbohydrate consumption via inhibition of pyruvate dehydrogenase (PDH), and over-activation of mTOR via elevated leucine levels (Li et al., 2017; Sun et al., 2016; Wang et al., 2016). However, relatively little is in fact known about the extent of BCAA oxidation by the heart, and whether it rises or falls with HF. It also remains unclear if the benefits of activating BCAA catabolism in HF are cardiac-autonomous or mediated via catabolism of BCAAs elsewhere.

The BCAA catabolic pathway is highly conserved across eukaryotes (Fig 1A). All three BCAAs are initially transaminated by branched-chain amino transferases (BCATs) to form branched chain alpha-ketoacids (BCKAs). The most common nitrogen acceptor is alpha-ketoglutarate, yielding glutamate. Two genes encode BCATs: BCAT1 (aka cBCAT) encodes a cytoplasmic protein and is primarily expressed in the brain. BCAT2 (aka mBCAT) encodes a mitochondrial protein and is ubiquitously expressed. Irreversible

and rate-limiting initiation of BCKA oxidation occurs in the branched-chain amino acid dehydrogenase (BCKDH) complex, found on the inner surface of the inner membrane of mitochondria. BCKDH catalyzes an oxidative decarboxylation, releasing CO_2 and covalently adding a Coenzyme A (CoA) group to the oxidized BCKA product. CoA, a bulky and hydrophilic prosthetic moiety, traps subsequent intermediates inside the mitochondria (with one exception: 3-hydroxyisobutyrate in the valine catabolic pathway). The large BCKDH complex has three components: a thiamin-dependent decarboxylase (E1), encoded by BCKDHA and B; a core multimeric dihidrolipoyl transacylase (E2), encoded by the DBT gene; and a dihydrolipoyl dehydrogenase (E3), encoded by DLD. The BCKDH complex is tightly regulated by phosphorylation/dephosphorylation. BCKDH kinase (BCKDK) phosphorylates and suppresses BCKDH activity, while the complementary activating dephosphorylation is carried out by the recently identified phosphatase, PPM1K (aka PP2Cm) (Lu et al., 2009). BCKDK is allosterically suppressed by BCKAs (greatest affinity for aKIC), thus allowing elevations in BCKAs to promote their own oxidation. After BCKDH decarboxylation, subsequent catabolism of BCAAs is largely unique to each BCAA, and all occur inside the mitochondrial matrix. Ultimately, all BCAA carbons are either lost as carbon dioxide or enter the TCA cycle (Figure 1A).

Here, we integrate studies with human heart failure cardiac tissues, newly generated mouse models of tissue-specific activation of BCAA catabolism, steady-state heavy isotope infusions, and population genetics, to evaluate in depth the role of BCAA catabolism in HF.

Results

Alterations in the BCAA pathway in failing human myocardium

To assess changes in the BCAA catabolic pathway that may occur in human heart failure (HF), we performed metabolomics on left ventricular tissue samples from explanted hearts of 40 patients with end-stage non-ischemic dilated cardiomyopathy and 49 organ donors without prior evidence of heart failure (non-failing, NF), combined with RNA-seq on a subset of these same samples (n = 14 and 17, respectively). Consistent with previous observations, we observed significantly increased levels of all three BCAAs and their respective BCKAs in HF compared to NF cardiac tissue (Figure 1A, S1A, Table S1) (Sun et al., 2016; Uddin et al., 2019). We also observed diminished expression of *BCKDHB* and *DBT*, as has been reported in rodent models of heart failure (Lai et al., 2014; Sun et al., 2016). These observations have suggested that failing myocardium is defective in BCAA catabolism (Sun et al., 2016; Uddin et al., 2019; Wang et al., 2016), and are consistent with a nearly 10-fold decrease in isovaleryl carnitine, a product of leucine oxidation (Fig 1A, S1A). However, numerous other catabolic products of leucine downstream of BCKDH, including 3-hydroxyisovaleric acid and methylgutaconic acid, were instead increased in failing human myocardium (Figure 1A, S1A), which is less consistent with a block at the BCKDH complex.

BCAAs enter and exit the cell via large neutral amino acid transporters LAT1 and LAT2 (comprised of SLC3A2 interacting with SLC7A5 or SLC7A8, respectively) and enter the mitochondria via SLC25A44 (Kanai et al., 1998; Segawa et al., 1999; Yoneshiro et al., 2019). RNA-seq analysis revealed significant downregulation of mRNA encoding all of

these transporters in failing heart (Figure 1A), suggesting a possible defect in BCAA transport in and out of the cell.

Using data from paired arterial and coronary sinus (CS) blood samples from patients with or without compensated heart failure (HF) (Murashige et al., 2020), we calculated the net uptake or release of BCAAs from the heart (Figure 1B). Whereas the non-failing heart consumes BCAAs, failing hearts tended to release BCAAs into the bloodstream. In parallel, using nitrogen balance as a surrogate for protein breakdown, we calculate a trend towards increased liberation of BCAAs from protein in failing compared to non-failing hearts (Figure S1C). Thus, there is a net increase in BCAA release from protein breakdown in failing hearts, but on average these BCAAs are secreted into the circulation rather than combusted in the heart. Overall, cardiac BCAA oxidation is quite low, contributing only to ~2% of total myocardial oxygen demand (Figure 1C). Together, these data indicate that cardiac pathways of BCAA transport and catabolism are significantly altered in human heart failure, but the data suggest that cardiac BCAA combustion may not, on balance, be suppressed in human heart failure.

Cardiac preference for BCAAs increases in murine heart failure

To measure directly cardiac BCAA catabolic flux in heart failure, we used steady-state heavy isotope infusions in mouse models of heart failure. Mice underwent sham or myocardial infarction (MI) surgery (by left anterior artery [LAD] ligation), and at 4 weeks post-surgery underwent infusions with a mixture of [U^{13}C]-labeled Leu, Ile, and Val (^{13}C-BCAA) in live, non-anesthetized animals for 120 minutes, followed by euthanasia and organ harvest (Figure 1D, Table S2). The rate of infusion was ~20% of endogenous circulatory turnover flux of each BCAA, and accordingly minimally perturbative. Hearts from mice subjected to MI surgery exhibited significantly dilated left ventricle (LV) with reduced LV ejection fraction (LVEF) and increased expression of canonical heart failure markers (Figure S1D–F and 1E). The failing hearts also exhibited significantly decreased expression of *Bckdhb* and *Dbt* and a trend towards decreased *Ppm1k* expression along with unchanged *Bckdk* expression (Figure 1F), consistent with previous findings in pressure overload-induced murine HF (Lai et al., 2014; Sun et al., 2016), and largely consistent with our findings in human heart failure (Figure 1A). We did not, however, observe alterations in BCAA catabolic enzyme levels or increased phosphorylation of BCKDHA at S293, as has been found previously (Figure 1G and S1G) (Wang et al., 2016).

In contrast to a previous study that observed diminished plasma BCAAs at the same time point post-MI (Wang et al., 2016), we observed a trend towards increased plasma BCAA levels in MI-treated animals, with no change in BCKAs (Figure 1H and S1H). In heart tissue, leucine was significantly increased after MI, and valine and isoleucine also trended higher (Figure 1I). All three BCAAs also trended higher in quadriceps after MI, while there was no change in liver (Figure S1I). The ^{13}C-BCAA infusions achieved steady-state labeling of plasma, at 15–20% ^{13}C enrichment of each BCAA, by 90 minutes of infusion (Figure IJ). Plasma enrichment of BCAAs was consistently lower in HF, despite identical body weights across groups (Figure S1J), reflecting >25% increase in whole-body circulatory turnover flux (F_{circ}) of BCAA carbon in MI-treated animals (Figure 1K). Relative incorporation of

BCAA-derived ^{13}C into intermediates of the TCA cycle in the heart revealed *increased*, rather than decreased, preference for BCAAs as a fuel in MI-treated hearts (Figure 1L). Increased BCAA oxidation was specific to the heart, as quadriceps demonstrated significantly decreased preference for BCAAs (Figure 1L) and liver showed no change (Figure S1K). Interestingly, the lower preference for BCAAs in quadriceps occurred in the absence of changes in mRNA expression of key enzymes, or phosphorylation of BCKDHA (Figure S1L–M).

Evaluation in an alternative model of HF, transverse aortic constriction (TAC), yielded similar results: the loss of contractile function after 8 weeks (Figure S1N) was accompanied by a trend towards cardiac BCAA accumulation with evidence of increased contribution of [U^{13}C]Ile to cardiac TCA intermediates (Figure S1O–P). In this milder model of HF, we observed no difference in total plasma BCAA level (Figure S1Q) or whole-body F_{circ} (Figure S1R–S) as well as more modest induction of cardiac *Anf* and *Bnp* expression (Figure S1T). Collectively these results indicate that failing hearts increase oxidation of BCAAs, that this occurs even in only mild HF, but that BCAAs remain only a minor heart fuel.

Global activation of BCAA catabolism improves cardiac remodeling pre- and post-myocardial infarction without affecting the choice of BCAAs as a fuel by the heart.—BT2 is a potent inhibitor of BCKDK, thereby enhancing BCKDH activity. Administration of BT2 to mice reduces plasma BCAA and BCKA within 30 minutes of injection, without affecting the endogenous rate of appearance of BCAAs (Neinast et al., 2019). Numerous groups have shown that daily administration of BT2, via injection or gavage, improves cardiac function 4–8 weeks post-injury in models of MI, TAC, and ischemia-reperfusion (Li et al., 2017; Sun et al., 2016; Wang et al., 2016). What remains unclear, however, is the mechanism by which activating BCAA catabolism benefits HF. The simplest explanation, generally assumed, is that cardiac oxidation of BCAAs is beneficial, and that BT2 administration promotes cardiac BCAA oxidation.

To test this notion, we used ^{13}C-BCAA infusions to investigate the effect of BT2 on systemic and tissue BCAA catabolism and levels after MI. Mice were administered BT2 in the chow (40 mg/kg/d, assuming typical food consumption), which achieved plasma BT2 levels comparable to those achieved with 40 mg/kg BT2 gavage (Figure S2A). 3 days after initiation of BT2 or control diet, mice underwent LAD ligation, and 4 weeks later the mice underwent steady-state ^{13}C-BCAA infusion (Figure 2A). BT2 achieved 20–25% and 30–40% reductions of fasting plasma BCAAs and BCKAs, respectively (Figure 2B), an effect comparable to that seen with administration of BT2 by gavage or injection (Sun et al., 2016; Wang et al., 2016). BCAAs in heart and skeletal muscle were lowered by 20–70% (Figure 2C and S2B). The expression of genes in the BCAA catabolic pathway was not altered by BT2 treatment (Figure S2C). As seen by others (Wang et al., 2016), administration of BT2 improved cardiac function 4 weeks after MI, improving both ejection fraction (EF) (Figure 2D) and cardiac dilation (Figure S2D). The post-MI ^{13}C-BCAA infusions achieved steady-state labeling of plasma, at 15–20% ^{13}C enrichment (Figure S2E). Plasma enrichment of BCAAs was indistinguishable between BT2-treated and control animals (Figure S2E), yielding nearly identical F_{circ} (Figure 2E). Relative incorporation of BCAA-derived ^{13}C into

intermediates of the TCA cycle in the heart and quadriceps revealed no differences between BT2-treated and control animals (Figure 2F and S2F). Thus, despite pronounced beneficial effects on cardiac function post-MI, and marked reductions in plasma and tissue BCAAs and BCKAs, BT2 had no apparent effect on cardiac BCAA oxidation.

In the above study, treatment with BT2 was started 3 days prior to MI, leaving open the possibility that treatment with BT2 prior to MI may reduce infarct size during the injury process. To address this question, we tested the effect of starting administration of BT2-containing chow 48 hours after MI instead of before MI (Fig 2G). 2 weeks post-MI, both BT2-treated and control groups revealed a similar extent of systolic dysfunction and ventricular dilation (Fig 2H–K). Over the ensuing 6 weeks, however, there was continuous improvement in all parameters in BT2-treated animals, with a 10% improvement in EF between treated and untreated groups by 8 weeks post-MI (LVEF 27% ctrl vs. 37% BT2, Figure 2I–K), and a trend to less weight gain (Figure S2G). Animals were sacrificed 8 weeks post-MI, revealing that administration of BT2 reduced heart weight/tibia length (HW/TL) and cardiac expression of markers of heart failure (*Anf, Myh7)* (Figure 2L–M). This study was duplicated in parallel at a separate institution (Temple University), similarly demonstrating significantly improved systolic function with BT2 administration initiated 2 days post-MI (Figure S2H). Surprisingly, in both of these studies, we observed no discernable difference in plasma BCAA level measured at the end of the experiments (Figure S2I and S2J). We also observed no apparent reduction in phosphorylation of cardiac BCKDHA S293, the target of BCKDK (Figure 2N). In line with this, we found that 1 week of BT2 treatment reduced liver BCKDHA S293 phosphorylation and promoted liver BCKDH complex activity, but did not reduce cardiac BCKDHA phosphorylation or significantly promote cardiac BCKDH dehydrogenase activity (Figure S2J–L). Finally, we did not find that BT2 significantly reduced phosphorylation of canonical mTORC1 pathway, known to be activated by leucine levels (Figure S2N). Together, these data demonstrate that BT2 potently protects from cardiac dysfunction post-MI, whether administered starting before or after ischemic injury, and that these protective effects may occur independently of changes in cardiac BCAA oxidation or plasma BCAA levels.

Activation of BCAA oxidation specifically in the heart does not confer cardiac benefit post-MI.—To formally test the role of cardiac BCAA oxidation in cardiac function and response to injury, we used CRISPR/Cas9 to generate new alleles of *Bckdk* in which exons 5–8 are flanked by Lox sites (Figure 3A and S3A–B). Exons 5–11 encode the catalytic activity of BCKDK, thus flanking exons 5–8 ensured loss of function with Cre-mediated recombination of the Lox sites. $Bckdk^{fl/fl}$ animals were then crossed with mice bearing a non-cardiotoxic *Myh6-Cre* transgene (Abel et al., 1999; Pugach et al., 2015) to generate cardiac-specific *Bckdk* knockout (BCKDK cKO) mice. cKO mice were born in Mendelian ratios and showed no difference in body weight or heart size, or plasma insulin or glucose level (Figure S3C–D). Hearts from BCKDK cKO demonstrated ~90% reductions in *Bckdk* mRNA and protein (Figure 3B–C), demonstrating efficient deletion and that nearly all cardiac BCKCK is found in cardiomyocytes. Phosphorylation of BCKDHA S293, the target of BCKDK, was significantly reduced in BCKDK cKO mice, and correlated with

extent of BCKDK deletion (Figure 3C). No compensation was noted in *Ppm1k* expression (Figure 3B).

To test the impact of loss of BCKDK on cardiac BCAA oxidation, BCKDK cKO and control animals were intravenously infused with [U^{13}C]isoleucine with unlabeled valine and leucine for 120 minutes (Figure 3D), achieving ~15% enrichment of cardiac isoleucine (Figure S3E). Consistent with previous estimates that BCAAs contribute to 2–3% of cardiac TCA carbons (Hui et al., 2020; Neinast et al., 2019) and our observations above (Figure 1J, 2F) cardiac oxidation of isoleucine was low (< 0.5% of TCA cycle carbon) in both groups. Enrichment of TCA intermediates was significantly higher in BCKDK cKO mice, demonstrating efficient activation of cardiac BCAA oxidation (Figure 3E). Strikingly, despite enhanced cardiac BCAA oxidation, BCKDK cKO mice did not have lower levels of cardiac BCAAs or BCKAs (Figure 3F) or plasma BCAAs (Figure S3F), indicating that rates of cardiac BCAA oxidation do not control cardiac BCAA levels. Consistent with the overall low contribution of cardiac BCAA oxidation to whole-body BCAA clearance, BCKDK cKO did not have accelerated clearance of orally administered BCAAs (Figure S3G).

To test the impact of increasing cardiac BCAA oxidation on cardiac response to injury, we first subjected mice to 2 weeks of isoproterenol infusion by osmotic pump. Both control and BCKDK cKO animals developed equivalent cardiac hypertrophy with the infusion protocol, indicating that increasing BCAA catabolism in the heart does not protect from pathologic cardiac hypertrophy (Figure 3G–I and S3H–J). Next, we subjected BCKDK cKO mice and littermate controls to MI via LAD ligation (Fig 4J). Plasma BCAAs were similar in both groups at 4 weeks post-MI (Figure S3J). We found no differences in mortality (Fig 3K), systolic function (Fig 3L), ventricular dilation (Fig 3M), or expression of genes associated with heart failure (*Anf, Bnp, Myh7*) or fibrosis (*Col1a1*) (Fig 3N) between the two groups. HW/BW and HW/TL ratios were not reduced in BCKDK cKO (Figure S3L–M). Phosphorylation of the canonical mTORC1 target eukaryotic initiation factor 4E-binding protein 1 (4E-BP1) was reduced in BCKDK cKO hearts post-MI (Figure S3O–P), but phosphorylation of ULK1 at Ser757 was not (Figure S3O). Collectively, these results indicate that promotion of cardiac BCAA oxidation does not prevent cardiac hypertrophy and does not prevent maladaptive cardiac remodeling following ischemic injury. Thus, from these data and those above, it appears that BT2 does not protect against HF by promoting cardiac-specific activation of BCAA catabolism.

Activation of BCAA oxidation in skeletal muscle is sufficient to lower plasma and cardiac BCAA and BCKA levels

From the above data, we reasoned that systemic activation of BCAA catabolism protects against HF not via direct action on the heart. We previously found that a single injection of BT2 induces BCAA catabolism most in skeletal muscle; that skeletal muscle is responsible for as much as 50% of whole-body BCAA catabolism; and that BCKDK is highly expressed in skeletal muscle (Neinast et al., 2019). We therefore sought to test the role of skeletal muscle BCAA oxidation in the response to cardiac ischemic injury.

Bckdk$^{fl/fl}$ animals were crossed with mice bearing a tamoxifen-inducible *Acta1-CreMCM* transgene (McCarthy et al., 2012) to generate inducible skeletal muscle-specific *Bckdk*

knockout (*Bckdk*$^{fl/fl}$ *ACTA1-CreMCM*$^{+/-}$, i.e. BCKDK iSkM KO) mice. Of note, this Cre driver mouse does not delete in the heart. BCKDK iSkMKO mice were born in Mendelian ratios and showed no evident abnormalities (Figure S4A). Immunobloting of extracts from quadriceps from BCKDK-iSkm KO revealed >95% reduction in BCKDK protein, compared to control (*Bckdk*$^{fl/fl}$ *ACTA1-CreMCM*$^{-/-}$) animals (Figure 4A and S4B), demonstrating efficient deletion and that nearly all skeletal muscle BCKDK is found in mature myofibers. Phosphorylation of BCKDHA S293 was reduced 50% in the BCKDK iSkMKO mice (Figure 4A and S4B). Steady-state intravenous infusion of ^{13}C-BCAAs showed that both groups achieved similar enrichment of circulating BCAAs with ^{13}C label, indicating that deletion of BCKDK in skeletal muscle does not affect whole-body BCAA circulatory turnover flux (i.e. rate of appearance of unlabeled BCAA from protein breakdown, (Figure 4B and S4C–D), similar to the lack of effect we observed on whole-body turnover flux by treatment with BT2 (Figure 2E). We did, however, find ~50% increase in ^{13}C enrichment of TCA cycle intermediates in quadriceps from BCKDK-iSkM KO relative to controls, demonstrating efficient activation of BCAA oxidation in skeletal muscle (Figure 4C). The increase in BCAA catabolism in skeletal muscle was accompanied by decreased BCAA and BCKA levels both in quadriceps and in plasma (Figure 4D–E), consistent with skeletal muscle, unlike heart, being a major whole body BCAA consumer. Levels of cardiac BCAAs were equivalently reduced (Figure 4F), indicating that plasma levels of BCAAs are likely a major determinant of cardiac levels, presumably due to rapid BCAA exchange between the circulation and cardiomyocytes. ^{13}C enrichment of TCA intermediates was decreased by ~40% in heart (Figure 4G), consistent with redistribution of whole-body BCAA catabolism towards skeletal muscle and away from other tissues, i.e. a “steal” phenomenon. These data demonstrate that skeletal muscle is a major site of BCAA oxidation; that activation of BCAA catabolism in skeletal muscle is sufficient to lower plasma and cardiac BCAA levels; and that plasma BCAA levels largely dictate cardiac levels.

Activation of BCAA oxidation specifically in skeletal muscle confers at most mild cardiac benefit post-MI.—To test the impact of increasing cardiac BCAA oxidation on cardiac response to injury, BCKDK-iSkM KO mice and littermate controls were subjected to MI by LAD ligation (Figure 4H–I). Survival in the short-term post-MI period trended to be reduced in the BCKDK-iSkM KO mice (Figure 4J), suggesting that lower plasma or cardiac BCAAs may worsen the acute tolerance to MI, although this was not seen with BT2 administration. Plasma levels at 4 weeks post-MI were reduced in BCKDK-iSkM KO mice (Figure S4E), to a similar extent as that achieved by BT2 administration (Figure 2B), and consistent with continued activation post-MI of BCAA catabolism in skeletal muscle. Of the surviving mice, there was no discernible difference between groups in LVEF by echocardiography at 2 weeks post-MI (Figure 4K). At 4 weeks post-MI, however, control mice trended to worsen LVEF compared to 2 weeks, while BCKDK-iSkM KO mice did not (Figure 4K). Both groups showed a similar degree of LV dilation at both time points (Figure 4L), and no differences were appreciated in heart weight/body weight or heart weight/tibia length ratios (Figure 4M and Figure S4F). Despite having decreased plasma and cardiac BCAA levels, there was no detectable decrease in cardiac mTORC1 activity in hearts of iSkM KO mice 4 weeks post-MI (Figure S4G). Cardiac expression of *Bnp* was mildly but significantly reduced in BCKDK-iSkM KO relative to

control mice (Figure 4N). Taken together, these data demonstrate that activation of BCAA catabolism specifically in skeletal muscle has at most a mild benefit on post-MI remodeling, which does not recapitulate the marked benefits seen with systemic activation of BCAA catabolism with BT2. Moreover, the mild observed benefit may reflect selection bias, as ~50% of BCKDK-iSkM KO mice died prior to 2-week and 4-week echocardiography, likely with worse, rather than better cardiac function compared to control mice. Thus, lowering plasma and cardiac BCAA levels to an extent similar to those seen with BT2 administration is not sufficient to provide cardiac protection equivalent to that seen with BT2 administration, suggesting alternative mechanisms of protection.

BT2 requires BCKDK to confer cardio-protection.—The observations that neither cardiac- nor skeletal muscle-specific deletion of BCKDK recapitulated the cardioprotective effects of BT2 raised the concern that BT2 may be targeting a protein other than BCKDK to confer cardio-protection. To test this possibility, we turned to whole-body *Bckdk*$^{-/-}$ mice, generated by crossing the *Bckdk*$^{fl/fl}$ mice with germline *Cmv-Cre* transgenic mice (Jackson Laboratory). Of note, this *Bckdk*$^{-/-}$ strain demonstrated growth retardation, epileptic seizures, and hindlimb clasping as reported previously (Joshi et al., 2006; Novarino et al., 2012). *Bckdk*$^{-/-}$ mice and +/+ controls were then subjected to MI by LAD ligation, followed by administration of BT2-containing diet starting 2 days post-MI (Figure 5A). Hearts from *Bckdk*$^{-/-}$ mice lacked any detectable BCKDK protein, or phosphorylation of BCKDHA S293 (Figure 5B). Interestingly, at baseline, hearts from *Bckdk*$^{-/-}$ had higher contractility than controls (% fractional shortening ~50% vs ~40%, Figure 5C) with no change in diastolic diameter or heart weight/tibia length ratio (Figure S5A–D). Plasma levels of BCAAs and BCKAs in *Bckdk*$^{-/-}$ mice were approximately 15–20% of control mice (Figure 5D), as reported previously (Neinast et al., 2019; Novarino et al., 2012), and were not further reduced by BT2 treatment, consistent with BT2 targeting BCKDK to affect plasma BCAA levels.

Bckdk$^{-/-}$ mice tolerated MI surgery well (Figure 5E). MI size was similar across groups (Figure 5F). Echocardiography performed at 4 weeks post-MI revealed that BT2 significantly improved LVEF and prevented ventricular dilation in control mice (Figure 5G–I), as we observed above (Figure 2). *Bckdk*$^{-/-}$ mice, in the absence of BT2 treatment, also revealed improved LVEF and ventricular dimensions post-MI compared to control mice (Figure 5G–I), consistent with the notion that global activation of BCAA catabolism, whether achieved pharmacologically with BT2 or genetically with deletion of BCKDK, may be sufficient to protect hearts post-MI, although it should be noted that *Bckdk*$^{-/-}$ mice had higher % fractional shortening at baseline (Figure 6C). Most importantly, BT2 treatment of *Bckdk*$^{-/-}$ mice did not improve cardiac function further, indicating that the cardioprotective effects of BT2 are most likely on-target, i.e. require the presence of BCKDK. Surprisingly, BT2 treatment of *Bckdk*$^{-/-}$ mice in fact reduced LVEF and worsened dilation in *Bckdk*$^{-/-}$ mice (Figure 5G–I). BT2 diet reduced HW/BW and HW/TL ratios in of *Bckdk*$^{+/+}$ animals, but increased HW/TL in *Bckdk*$^{-/-}$ animals (Figure 5J–K). Expression of HF-associated markers *Anf* and *Bnp* tended to be decreased in *Bckdk*$^{+/+}$ treated with BT2, but were not reduced in *Bckdk*$^{-/-}$ given BT2 diet (Figure S5G–H). Together, these data show: 1) that global activation of BCAA catabolism is cardioprotective, be it acute or lifelong; 2) most

importantly, that the cardioprotective effects of BT2 require the presence of BCKDK, i.e. are on target; and 3) that BT2 also has off-target effects that worsen cardiac function, potentially antagonizing its BCKDK-dependent cardioprotective effects.

Global activation of BCAA catabolism promotes vasodilation and lowers blood pressure.—The observations that neither cardiac- nor skeletal muscle-specific deletion of BCKDK recapitulated the cardioprotective effects of BT2, and that the latter do occur via targeting BCKDK, suggested that cardioprotection is conferred by suppressing BCKDK elsewhere. BT2 has been shown to be cardioprotective after a wide range of cardiac insults, including pressure overload, myocardial infarction, and ischemia/reperfusion. One potential mechanism to explain benefit in these disparate contexts is micro- or macro-vascular dilation, a well-established cardioprotective mechanism. To investigate this possibility, we measured arterial blood pressure (BP) via invasive hemodynamics in wildtype animals after administration of BT2-containing chow, versus control, for 7 days (Figure 6A). Strikingly, BT2 lowered systolic, diastolic, and mean arterial BP by ~10mmHg in WT (Figure 6B). Endothelial release of NO by eNOS is a dominant mechanism of BP control (Förstermann et al., 2018; Rapoport et al., 1983), and inhibition of eNOS with N^G-Nitro-L-arginine-methyl-ester (L-NAME) is sufficient to increase BP (Lahera et al., 1991). Even in the presence of L-NAME, however, BT2 significantly lowered BP (Figure 6C–D), indicating that global activation of BCAA catabolism can lower BP by a mechanism other than promoting NO production by eNOS. Similar findings were observed when monitoring live and undisturbed mice with implanted telemetry devices over the span of 4 weeks: BT2-containing chow lowered BP by ~7–10mmHg, in both awake and sleeping cycles, and did so even when co-administered with L-NAME (Figure 6E–F and S6A–C). Administration of low-BCAA diet to mice for 1 week raised BP, measured by continuous telemetry, by ~5mmHg (Figure S6D), supporting the conclusion that BCAA homeostasis impacts BP regulation, and suggesting that the effects of BT2 on BP are likely mediated by increasing BCAA oxidation, rather than by reducing plasma BCAA levels. BT2 had no effect on BP in whole-body BCKDK$^{-/-}$ mice (Figure S6E), indicating that BT2 likely acts on-target to lower BP.

To test if the effects of BT2 on BP were mediated by the vasculature, we isolated carotid vessels from animals administered BT2-containing chow, versus control, and subjected the vessels to ex vivo measurements of contractility and relaxation. Preconditioning of the vessels with 40–80 mmHg luminal pressures led to equivalent dilation between groups (Figure 6G). However, after vasoconstrictive treatment with phenylephrine (PE), the vessels from BT2-treated animals remained markedly more dilated (Figure 6G–H). In contrast, the ability of acetylcholine (Ach), an activator of eNOS, to dilate the vessels was not statistically different between groups (Figure 6I), consistent with vasodilatory effects of BT2 that are independent from NO. These data demonstrate that global activation of BCAA oxidation lowers BP, and does so likely via vascular desensitization to adrenergic signaling, which is in turn cardioprotective.

Mendelian Randomization studies support a causal relationship between BCAAs and blood pressure in human cohorts.—In light of the observation that

global activation of BCAA oxidation reduces blood pressure in experimental animals, we interrogated via Mendelian Randomization (MR) the relationship between genetic propensity for elevated plasma BCAAs and blood pressure in human cohorts. MR is a form of instrumental variable analysis, which uses genetic proxies to simulate a randomized controlled trial, estimating the effect of an exposure (in this case BCAA) on an outcome of interest (in this case blood pressure traits). For the primary analysis, genetic variants associated with BCAA were identified from metabolomics analyses from Kettunen et. al. (Kettunen et al., 2016). Inverse variance-weighted MR was performed to test the association between circulating BCAA and systolic blood pressure (SBP), diastolic blood pressure (DBP), mean arterial pressure (MAP), and pulse pressure (PP), assessed among participants of UK Biobank (UKB). Robust associations were observed between increased leucine, as well as isoleucine, and increased SBP, as well as PP, after correction for BMI and diabetes status (Figure 7A). In a second sensitivity analysis, the genetic instruments for BCAA levels were instead derived among ~115k participants of UKB, and associations between BCAA levels and BP traits were then assessed using SBP and DBP from the International Consortium on Blood Pressure (ICBP)+UKB GWAS meta-analysis (Evangelou et al., 2018). Significant associations were again observed between increased BCAAs, individually or pooled, and increased SBP (Figure S7).

44 variants, in 26 genetic loci, were identified in total as associated with a BCAA plasma level across either the Kettunen et al. or UKB cohorts (Table S3). Of these 26 loci, 7 were located within 500kb of one of 14 pre-determined genes unique to the BCAA catabolic pathway (Table S4), representing a highly significant enrichment compared with matched loci (one-tailed permutation $p < 1 \times 10^{-4}$). Reasoning that these SNPs may be less pleiotropic, we re-evaluated the MR analysis using these more restrictive genetic instruments. In this sensitivity analysis, previous associations further increased in significance, and significant associations were now apparent between elevations of each of the three BCAAs and increases in all of the blood pressure parameters, i.e. DBP, SBP, MAP, and PP (Figure 7B). Together, these data demonstrate that exposure to genetic predisposition for increased BCAA levels, in particular due to SNPs. near genes unique to BCAA catabolism genes, associates strongly with increased blood pressure in large human cohorts. The data thus strongly support the notion that modulation of BCAA catabolism affects blood pressure in humans.

Discussion

BCAAs have recently gathered broad attention as potential contributors to heart failure. We make here a number of new observations that reevaluate the underlying mechanism. First, it has been widely assumed, based largely on gene expression studies and studies of whole-body modulation of BCAA catabolism, that heart failure is accompanied by suppressed oxidation of BCAAs in the heart. We show here, however, that BCAA oxidation is in fact likely not suppressed in heart failure. We support this conclusion with data from both humans and mice, measuring A/V differences across the human heart, and *in vivo* steady-state isotopic studies in mice, both direct measures of cardiac BCAA flux. The discrepancy between the observed transcriptional suppression of BCAA catabolic genes in heart failure and the observed unchanged, or indeed possibly even increased, cardiac

oxidation of BCAAs in heart failure reflects the important fact that enzyme abundance is just one of many variables impacting metabolic flux. In the case of BCAA oxidation, for example, other factors may include redox state, post-translational modifications, sub-cellular localization, substrate abundance, product inhibition, and allosteric regulation. Thus, defective cardiac oxidation of BCAAs is unlikely to contribute to heart failure progression.

Despite this conclusion, it is clear that systemic activation of BCAA oxidation with BT2 protects from maladaptive remodeling in heart failure, at least in murine models. This is true in multiple models of heart failure, including hemodynamic and ischemic models, as shown by multiple independent groups (Chen et al., 2019; Li et al., 2017; Sun et al., 2016; Wang et al., 2016). We also show here that initiating treatment with BT2 after ischemic insult is as effective as before insult, indicating that BT2 improves post-infarct maladaptive remodeling, rather than, for example, reducing infarct size in the 24 hours after insult. Importantly, we also show genetically that BT2 acts on-target, i.e. via suppression of BCKDK, indicating that cardioprotection is indeed conferred by modulation of BCAA metabolism. There is thus little doubt that systemic activation of BCAA catabolism is cardioprotective, and an appealing new target for drug development.

The mechanism of cardioprotection, however, has remained unclear. Studies to date have assumed that the potent cardioprotective effect of BT2 is mediated via increasing cardiac BCAA oxidation. All studies to date, however, have used whole-body modulation of BCAA oxidation, be it pharmacological (BT2) or genetic (PPM1K knockout animals), leaving untested which tissues contribute to cardioprotection. We show here that BT2-mediated cardioprotection does not occur via increased cardiac BCAA oxidation. BT2 does not increase cardiac BCAA oxidation in vivo. Moreover, cardiac-specific deletion of BCKDK –modeling cardiac-specific BT2 treatment – fails to recapitulate the benefits of whole-body BCKDK suppression. We conclude that BCAA oxidation in a tissue other than the heart has profound effects on progression of heart failure.

One model to explain cardioprotection via activation of extra-cardiac BCAA oxidation invokes consequent reduced levels of cardiac BCAA and BCKA levels. Indeed, we show here that cardiac BCAA levels are largely dictated by plasma levels, rather than cardiac-specific BCAA metabolism, consistent with our prior observations of rapid exchange of BCAAs across the plasma membrane (Neinast et al., 2019). Decreased cardiac BCAA and BCKA levels have been proposed to disinhibit PDH (Li et al., 2017), reduce ROS production (Sun et al., 2016), reduce protein synthesis (Walejko et al., 2021), and relieve mTOR activation and inhibition of autophagy (Wang et al., 2016). However, our data show that lowering systemic and cardiac levels of BCAAs or BCKAs via skeletal muscle BCKDK KO confers at most mild cardioprotection, indicating the existence of other mechanisms of protection conferred by systemic activation of BCAA oxidation.

In our search for alternative mechanisms, we discovered that, surprisingly, BCAAs affect blood pressure. Pharmacological activation of BCAA oxidation lowers blood pressure in rodents, and Mendelian randomization studies link BCAAs to blood pressure in humans. Epidemiological relationships between BCAAs and blood pressure have been noted recently: Dullaart et al measured plasma BCAAs in subjects of the PREVEND study, and

found that elevated BCAAs at entry into the study correlated strongly with subsequent incident hypertension (HR 1.30 per 1SD increment of BCAA levels, p<0.001) (Flores-Guerrero et al., 2019), and Tanabe et al. performed a case-control plasma metabolomic study of 1250 subjects with hypertension vs 1250 normotensive controls and identified BCAAs levels as most strongly associated with hypertension (Mahbub et al., 2020). Our mouse interventional studies and human Mendelian randomization studies indicate that aberrant BCAA metabolism is likely causal to elevated BP, at least in part explaining these correlative epidemiological observations.

Mechanistically, we find that BCAA oxidation modulates vascular tone, in particular the vascular response to adrenergic tonicity. Importantly, the effects are at least in part independent of signaling by NO derived from endothelial cells. It is thus likely that BCAA oxidation in smooth muscle cells (SMCs) is responsible for modulating vascular tone and blood pressure. Modulation could also occur indirectly, for example through central mechanisms. Further studies will be required to understand if and how BCAA oxidation in SMCs modulates calcium or cAMP signaling or other downstream effects of adrenergic stimulus. It will also be of interest to determine if activating BCAA oxidation only in SMCs is sufficient to affect blood pressure.

Activation of BCAA oxidation has been shown to be cardioprotective after a wide range of cardiac insults, including pressure overload, myocardial infarction, and ischemia/reperfusion (Li et al., 2017; Sun et al., 2016; Wang et al., 2016). The surprising effect of BCAA oxidation on vasorelaxation, a well-established cardioprotective mechanism, provides a potential explanation for the benefits of activating systemic BCAA oxidation across multiple distinct models of heart failure. The cardioprotective mechanisms may differ between different cardiac insult paradigms. For example, afterload reduction may explain cardioprotection in the context of myocardial infarction, but is less likely to do so in the context of pressure overload, where afterload is artificially elevated. In the latter case, protection may be afforded by other vasodilatory effects, for example coronary vascular dilation and improved cardiac tissue perfusion. Other tissues may also contribute. It will be of future interest to compare, or superimpose, BT2 or BT2-like drugs to existing regimens of vasorelaxation and lowering blood pressure (e.g. beta blockade or RAAS inhibition).

In summary, we show here: that BCAA oxidation in cardiac tissue is not suppressed in the context of heart failure, contrary to current thinking; that the strong cardioprotection conferred by pharmacological activation of BCAA oxidation is mediated by extra-cardiac tissues; that lowering plasma BCAA levels is not sufficient to fully explain the cardioprotection afforded by systemic activation of BCAA oxidation; and, surprisingly, that BCAA oxidation regulates vascular tone and blood pressure, potentially explaining at least in part the observed cardioprotection. The BCAA pathway is eminently targetable for therapeutic purposes, as demonstrated by BT2 itself. Our work demonstrates that BCKDK is indeed the relevant therapeutic target *in vivo*, and provides mechanistic insight to assist in the development of this target for therapy in heart failure.

Limitations

Our study has several limitations. Most studies are performed in mouse models, and extrapolations to human heart failure must be cautious. Although our studies introduce the surprising finding, in mice and humans, that BCAA oxidation modulates BP, the precise molecular mechanism remains to be elucidated. In addition, although our studies strongly suggest afterload reduction and increases in myocardial perfusion as explanations for the cardioprotective effect of BT2, formal proof of this causal relationship will require understanding and modulating the mechanism by which BT2 affects vascular reactivity.

STAR Methods

RESOURCE AVAILABILITY

Lead contact

- Further information and requests for resources and reagents should be directed to and will be fulfilled by the lead contact, Zoltan Arany (zarany@pennmedicine.upenn.edu).

Materials availability

- Mouse lines generated in this study are available upon request to lead contact.
- This study did not generate new unique reagents.

Data and code availability

- All RNAseq data are publicly available in the NCBI GEO repository under the accession identifier listed in the key resources table GSE14190.
- Human tissue and plasma metabolomics data have been deposited to the EMBL-EBI Metabolights database and are publicly available under the accession identifier listed in the key resources table.
- All original code related to Mendelian randomization has been deposited at Zenodo and is publicly available under the accession identifier listed in the key resources table.
- Code related to RNAseq analyses was reported previously *Flam et al.* 2022 and is available upon request (Flam et al.)
- Any additional information required to reanalyze the data reported in this paper is available from the lead contact upon request.

EXPERIMENTAL MODEL AND SUBJECT DETAILS

Mice—Animal studies were approved and carried out in accordance with the University of Pennsylvania's Institutional Animal Care and Use Committee (IACUC). All mice were maintained in 12h:12h light-dark cycle under standard temperature and humidity, and had *ad libitum* access to food and water. Care and handling of animals were in accordance with the guidelines of the UPenn IACUC. For generation of *Bckdk*$^{fl/fl}$ line, loxP sites

were inserted in introns between exons 4 and 5 and between exons 8 and 9. CRISPR components (Cas9 mRNA, gRNA × 2 and ssODN donors × 2) were delivered into one-cell stage zygotes (B6SJL/F1 background) via microinjection. Cardiac-specific BCKDK KO mice were created by crossing *Bckdk*$^{fl/fl}$ to *αMHC-Cre*, which was generated in an FVB background (Abel et al., 1999).

Breeding pairs of *Bckdk*$^{fl/fl}$ *αMHC-Cre*$^{-/-}$ with *Bckdk*$^{fl/fl}$ *αMHC-Cre*$^{+/-}$ yielded litters in the expected mendelian ratio. Tamoxifen-inducible skeletal muscle BCKDK KO mice were created by crossing *Bckdk*$^{fl/fl}$ to *HSA-Cre*, which was generated in a C57Bl6 background (Jackson Laboratory Strain #025750, (McCarthy et al., 2012)). Breeding pairs of *Bckdk*$^{fl/fl}$ *HSA-Cre*$^{-}$ with *Bckdk*$^{fl/fl}$ *HSA-Cre*$^{+}$ yielded litters in the expected mendelian ratio. To induce deletion, mice (4–8 weeks of age) were given tamoxifen-containing diet (400 mg Tamoxifen/kg diet; Envigo TD.130859) for 3 weeks, followed by a 2-week washout period where they were given standard chow (Purina LabDiet 5010). Whole-body BCKDK KO mice were generated by crossing *Bckdk*$^{fl/fl}$ to *CMV-cre* (B6.C-Tg(CMV-cre)1Cgn/J; The Jackson Laboratory 6054) to generate whole-body *Bckdk*$^{+/-}$, which were then crossed to generate *Bckdk*$^{+/+}$ and *Bckdk*$^{-/-}$ breeding pairs. Progeny from *Bckdk*$^{+/+}$ × *Bckdk*$^{+/+}$ and *Bckdk*$^{-/-}$ × *Bckdk*$^{-/-}$ breeding pairs whose progeny were then used for MI studies. Breeding pairs of *Bckdk*$^{-/-}$ × *Bckdk*$^{-/-}$ were fed a 2X-BCAA “breeding diet”(OpenStandard Diet with 2X BCAA, Research Diets Inc.), as whole-body *Bckdk*$^{-/-}$ females were infertile on standard chow. *Bckdk*$^{+/+}$ × *Bckdk*$^{+/+}$ breeding pairs were fed a matching control diet (OpenStandard Diet with 1X BCAA, Research Diets Inc.). For the experiments shown in Figures 2, 3, and 7 (except BCKDK$^{-/-}$ in Figure S7E), C57Bl6J mice were purchased from Jackson Laboratories (Stock 664).

Human myocardial and plasma samples: RNAseq, cardiac/plasma metabolomics—The study protocol was approved by the Institutional Review Board of the Hospital of the University of Pennsylvania. All study participants provided written informed consent. All patients were >18 years of age and non-pregnant. Both males and females were included; details regarding age and sex of participants can be found in Supplemental Table 1. We performed our studies in two cohorts. The first cohort of n=18 end-stage failing and n=18 non-failing hearts was matched for age, gender, and race. Non-failing status was determined by ejection fraction (EF) ≥ 50% with no history of HF. All failing hearts were diagnosed as non-ischemic cardiomyopathy or dilated cardiomyopathy with no coronary artery disease (CAD) or sarcoidosis etiology. Patients with a history of diabetes or left ventricular assist device (LVAD) were excluded from both populations. The second cohort of 30 NF and 21 HF samples was chosen within the same criteria as the first, but without gender and race matching. All samples were used for human tissue metabolomics analysis. A subset of these were used for genome-wide RNAseq expression data (n=17 nonfailing and 14 DCM hearts).

Human paired arterial and coronary sinus samples—Patient cohort and method details are as reported in Murashige et al. 2020 (Murashige et al., 2020). All patients were undergoing elective radiofrequency catheter ablation for treatment of atrial fibrillation or ventricular tachycardia. The study protocol was approved by the Institutional Review Board

of the Hospital of the University of Pennsylvania (Federalwide Assurance #00004028, Board #1 Protocol #827174). All study participants provided written informed consent. All patients were >18 years of age and non-pregnant. All patients had fasted overnight and were under general anesthesia with propofol, remifentanil, etomidate, and succinylcholine. Following induction of general anesthesia, a 20-gauge catheter was inserted into the radial artery to continuously monitor blood pressure. Hemostatic sheaths were inserted into the femoral veins. One of these sheaths was exchanged for a long SL0TM sheath (Abbott, Chicago, IL) which was advanced over a diagnostic catheter into the coronary sinus. Within 60 minutes of induction of anesthesia, samples were simultaneously drawn from the radial artery, femoral vein, and coronary sinus. All blood samples were drawn prior to initiation of ablation. Mean right and left atrial chamber pressures were measured immediately prior to and following transseptal puncture and are reported as the average of the two measurements recorded by the two transseptal sheaths. Echocardiographic findings are reported from the most recent echocardiogram done prior to procedure. Blood samples were collected in lithium-heparin treated vacutainers and placed immediately on ice. Plasma was separated by centrifugation at 3,000g at 4°C for 10 minutes, and all samples were stored at −80°C until analysis. Blood oxygen content was measured in arterial, coronary sinus, and femoral venous samples of 17 patients at the time of sample collection using an ABL90 FlexPlus blood gas analyzer (Radiometer, Brea, CA).

METHOD DETAILS

Quantification of Arterial-Coronary Sinus BCAA gradient and cardiac BCAA combustion in human heart—For amino acids, the concentration of metabolite consumed was calculated based on the net combustion of each amino acid as calculated below. Cardiac amino acid release from proteolysis was calculated using the net amino acid A-V nitrogen balance across the heart of each patient as originally reported in (Murashige et al., 2020) and the average overall amino acid composition of muscle protein (Clowes et al., 1980; Hall et al., 1999; Pisarenko et al., 1986; Taegtmeyer et al., 1977; Takala et al., 1980). For all calculations, each patient's measured concentration of Ile, Leu, and Val was used.

The net A-V nitrogen balance from amino acid uptake and release was calculated for each patient according to:

$$\Delta N_{A.A.} = \sum([N_{A.A.}]_{C.S.} - [N_{A.A.}]_{Art})$$

where $N_{A.A.}$ represents total amino acid nitrogen concentration. For a given amino acid i ($A.A._i$), the net uptake or release of $A.A._i$ is dictated by the net liberation of $A.A._i$ from proteolysis and net metabolic combustion of $A.A._i$:

$$\Delta[A.A._i]_{AV} = [A.A._{i.}]_{C.S.} - [A.A._i]_{Art}$$

$$\Delta[A.A._i]_{AV} = [net\ liberation\ of\ A.A._{i.}\ \ from\ protein] - [net\ combustion\ of\ A.A._{i.}]$$

The net liberation of $A.\ A._i$ from protein was calculated using the net amino acid A-V nitrogen balance and the typical composition of muscle protein using the following:

$$\text{net liberation of } A.A._i \text{ from protein } = a_i\left(\frac{\Delta N_{A.A.}}{k}\right)$$

where a_i is the abundance of amino acid i in protein and k is the average weighted nitrogen content per amino acid in myocardial protein. A value of $k = 1.38$ was used here. Thus, net myocardial combustion of $A.\ A._i$:

$$\text{net combustion of } A.A._i = a_i\left(\frac{\Delta N_{A.A.}}{k}\right) - \Delta[A.A._i]_{AV}$$

Predicted oxygen requirements for substrate catabolism were based on theoretical full oxidation of metabolites that were consumed by the heart:

$$C_aH_bO_cN_d + xO_2 \rightarrow CO_2 + H_2O$$

RNAseq—RNA sequencing libraries were prepared using the Illumina TruSeq stranded mRNA kit followed by the Nugen Ovation amplification kit. To avoid confounding by batch effects, libraries were randomly selected into pools of 32, and pools were sequenced on a Hiseq2500 to a depth of ~30 million 100-bp paired-end reads per biological sample. Fastq files were aligned against human reference (hg19/hGRC37) using the STAR aligner. Duplicate reads were removed using MarkDuplicates from Picard tools, and per gene read counts for Ensembl (v75) gene annotations were computed. Expression levels in counts per million (CPM) were normalized and transformed using the VOOM procedure in the LIMMA R package. Surrogate variables to account sources of latent variation such as batch were calculated using the svaseq function from the SVA package.

RNA extraction, cDNA synthesis, and qRT-PCR—Aliquots of pulverized frozen tissue were placed in homogenization tubes on ice with 5–6 ceramic beads. 1 mL cold TRIzol lysis reagent (ThermoFisher 15596026) was added to each sample. Samples were then homogenized in a bead homogenizer (Omni International) for two cycles of 20 seconds separated by a 10-second pause. Total RNA was then isolated following manufacturers instructions. Samples were then reverse transcribed using Applied Biosystems High-Capacity cDNA Reverse Transcription Kit according to instructions (ThermoFisher 4368813). Quantitative real-time PCR was performed on the cDNAs in the presence of fluorescent dye (SYBR green, BioRad) using primers listed in Supplemental Table 6. Expression levels were determined using the comparative cycle threshold ($2^{-\Delta\Delta Ct}$) method.

Metabolite extraction—Serum (5 μL) was mixed with 150 μL −20°C 40:40:20 methanol:acetonitrile:water (extraction solvent), vortexed, and immediately centrifuged at 16,000 × g for 10 min at 4°C. The supernatant was collected for LC-MS analysis. To extract metabolites from heart samples, frozen hearts were ground at liquid nitrogen temperature with a Cryomill (Retsch, Newtown, PA). The resulting tissue powder (~20 mg) was

weighed and then extracted by adding −20°C extraction solvent (as above), vortexed, and immediately centrifuged at 16,000 × g for 10 min at 4°C. The volume of the extraction solution (μL) was 40x the weight of tissue (mg) to make an extract of 25 mg tissue per mL solvent. The supernatant was collected for LC-MS analysis.

Metabolite measurement by LC-MS—A quadrupole-orbitrap mass spectrometer (Q Exactive, Thermo Fisher Scientific, San Jose, CA) operating in negative ion mode was coupled to hydrophilic interaction chromatography via electrospray ionization and used to scan from m/z 70 to 1000 at 1 Hz and 140,000 resolution. LC separation was on a XBridge BEH Amide column (2.1 mm × 150 mm, 2.5 μm particle size, 130 Å pore size; Waters, Milford, MA) using a gradient of solvent A (20 mM ammonium acetate, 20 mM ammonium hydroxide in 95:5 water: acetonitrile, pH 9.45) and solvent B (acetonitrile). Flow rate was 150 μL/min. The LC gradient was: 0 min, 85% B; 2 min, 85% B; 3 min, 80% B; 5 min, 80% B; 6 min, 75% B; 7 min, 75% B; 8 min, 70% B; 9 min, 70% B; 10 min, 50% B; 12 min, 50% B; 13 min, 25% B; 16 min, 25% B; 18 min, 0% B; 23 min, 0% B; 24 min, 85% B; 30 min, 85% B. Autosampler temperature was 5°C, and injection volume was 3 μL. Data were analyzed using the MAVEN software (Melamud et al., 2010).

BCKDH complex activity assay—To measure BCKDH complex activity, approximately 50 mg of frozen tissue were homogenized (Bead ruptor 12, OMNI international) in 1200 μl of ice-cold extraction buffer (50 mM HEPES, 3% (w/v) Triton X-100, 2 mM EDTA, 5 mM dithiothreitol (DTT), 0.5 mM thiamine pyrophosphate, 50 mM potassium fluoride, 2% (v/v) bovine serum, 0.1 mM *N*-tosyl-L-phenylalanine chloromethyl ketone, 0.1 mg/ml Trypsin inhibitor, 0.02 mg/ml leupeptin, phosphatase inhibitor (Roche), pH7.4 at 4°C adjusted with KOH). Extracts were cleared by centrifugation at 4°C, 12,000 × *g* for 10 minutes. To the supernatant, 600 μl of 27% (wt/vol) PEG-600 was added and incubated for 20 minutes on ice. Precipitated protein was centrifuged (12,000 × *g*, 10 minutes at 4°C) and resuspended in 1 ml of suspension buffer (25 mM HEPES, 0.1% (w/v) Triton X-100, 0.2 mM EDTA, 0.4 mM thiamine pyrophosphate, 1 mM DTT, 50 mM KCl, 0.02 mg/ml leupeptin, phosphatase inhibitor (Roche), pH7.4 at 37°C adjusted with KOH). Protein concentration was normalized using Bradford assay (Biorad). Normalized samples (60 μl) were diluted with sterile water (40 μl) and assay buffer (100 μl, 60 mM potassium phosphate, 4 mM $MgCl_2$, 0.8 mM thiamine pyrophosphate, 0.8 mM CoA, 2 mM NAD+, 0.2% (w/v) Triton X-100 and 4 mM DTT pH7.3 at 30°C adjusted with KOH) in a 96 well polystyrene plate. Before adding to the samples, sterile water and assay buffer was prewarmed to 30°C. Absorbance 340 nm at 30°C was recorded for 10 minutes to establish a stable baseline. To initiate the reaction, pre-warmed (30°C) 10 mM α-ketoisovalerate (final concentration 1 m*M*) was added and absorbance was measured every minute for 70 minutes. For each reading, absorbance 650 nm was subtracted for absorbance baseline correction. The method was adopted from Nakai et al, 2000 and Webb et al, 2019 (Nakai et al., 2000; Webb et al., 2019).

BCAA tolerance test—Mice were starved for 5 hours (8:00 am ~1:00 pm) and orally administered with BCAA solution. BCAA solution was formulated with 60 mM valine, 82.5 mM leucine, 37.5 mM isoleucine according to natural abundance ratio (1.6 (Val):2 (Leu):1 (Ile)) in saline and 8 ml was injected for every gram of mouse body weight. Blood

was collected from tail at 8, 30, 60 minutes after injection. Blood sample was centrifuged at 10,000 × g, 4°C for 15 minutes and plasma was collected for gas chromatography/mass spectrometry (GC (Agilent, 7890)/MS (Agilent, 5977B)) analysis. Briefly for GC/MS analysis, metabolite was extracted from 10 ml of serum using methanol and dried using vacuum centrifugation. Dried metabolites were derivatized with 50 (N-Methyl-N-tert-butyldimethylsilyltrifluoroacetamide): 50 (Acetonitrile) at 70 °C for 90 minutes. Derivatized samples were cleared with centrifugation and loaded on the sample vial for GC/MS analysis.

Administration of isoproterenol by osmotic pump—Isoproterenol (Sigma-Aldrich I6504) was dissolved in sterile saline (197 mg isoproterenol/1 mL saline) and continuously delivered via subcutaneous osmotic pump (Alzet 1002, DURECT corporation, Cupertino, CA) for 14 days at a target dose of 30 mg isoproterenol/kg/day.

Surgical heart failure models—Mice were anesthetized with ketamine (100 mg/kg) and xylazine (10 mg/kg) and acepromazine (2mg/kg) (administered intraperitoneally. To perform either TAC or MI surgery, mice were restrained supine, intubated, and ventilated using a Harvard respirator. For TAC: following dissection through the intercostal muscles, the aorta was identified and freed by blunt dissection. 7.0 silk suture was placed around a 27-gauge needle, suture was tied, and needle removed. For MI surgery, a left thoracotomy. Was performed, the LV and the left main coronary artery system exposed, and the mid-LAD ligated with a 8–0 silk suture. The surgical incision was closed, and the mice were recovered on a warmer until being returned to their cage.

Echocardiographic studies—Ultrasound examination was performed using a Vevo 2100 Ultrasound System (VisualSonics Inc, Toronto, Ontario, Canada). Mice were lightly anesthetized with an I.P. injection of 0.005 ml/g of 2% Avertin (2,2,2-Tribromoethanol, Sigma-Aldrich, St. Louis, MO). Hair was removed from the anterior chest using chemical hair remover, and the animals were placed on a warming pad in a left lateral decubitus position to maintain normothermia (37°C). Ultrasound gel was applied to the chest. Care was taken to maintain adequate contact while avoiding excessive pressure on the chest. Two-dimensional images were obtained by hand-held manipulation of the ultrasound transducer. Complete 2-D long-axis and Doppler ultrasound examination of the TAC gradient (where applicable) were performed using multiple views. After completion of the imaging studies mice were allowed to recover from anesthesia and returned to their cages. To ensure consistent infarct sizes across groups, all mice underwent a screening echocardiogram at 1.5–2 weeks post-MI by a blinded investigator. Those mice with a very small MI (i.e. minimal or no regional wall motion abnormality) or a very large MI (i.e. akinetic ventricle) were excluded from further analysis.

Infusion of BCAAs in Mice—Animal studies followed protocols approved by the University of Pennsylvania Institutional Animal Care and Use Committee. The mice were on normal light cycle (7AM-7PM). *In vivo* infusion was performed on 10–14 week old male C57Bl/6J mice (The Jackson Laboratory 664) with a catheter surgically implanted in the right jugular vein. Infusion was performed for 2 hours to achieve isotopic steady state. The mouse infusion setup (Instech Laboratories, Plymouth Meeting, PA) included

a tether and swivel system so that the animal has free movement in the cage with bedding material and free access to water. A mixture of ^{13}C-labeled BCAAs (Cambridge Isotope Laboratories, Tewksbury, MA) or ^{13}C-isoleucine + unlabeled BCAAs depending on experiment was prepared as solution in normal saline and infused via the catheter at 0.1 uL/g/min. Blood samples were collected by tail bleeding in lithium-heparin coated tubes (Sarstedt 16.443.100), placed on ice, and centrifuged at 16,000 × 6 for 10 min at 4 C. For tissue harvest, mice were euthanized with pentobarbital injection followed by cervical dislocation. Tissues were quickly dissected and frozen in liquid nitrogen with a pre-cooled Wollenberger clamp. Serum and tissue samples were kept at −80 C until further analysis.

Western Blots—Tissues were lysed in RIPA buffer containing phosphatase and proteinase inhibitors (PhosSTOP and Complete miniproteinase inhibitor cocktail, Roche). Protein concentration was quantified by BCA protein assay kit (Thermo Fisher Scientific), and the same amount of protein (10–20 ug) was loaded in a 4%–20% gradient Tris-glycine polyacrylamide gel (Bio-Rad) and electrophoresed (SDS-PAGE). After the SDS-PAGE, protein samples were transferred to PVDF membrane (Millipore). Membranes were blocked by 5% skim milk for 1 h and then incubated with the respective primary antibodies: BCKDK (abcam ab128935, RRID:AB_11142023), phospho-BCKDHa S293 (Bethyl, A304–672A, RRID:AB_2620867), total BCKDHA (Bethyl A303–790A, RRID:AB_11218185), ß-Tubulin (Cell Signaling 2128, RRID:AB_823664), GAPDH (Cell Signaling 2118, RRID:AB_561053), 14-3-3 (Cell Signaling 9636, RRID:AB_560823). Appropriate HRP-conjugated secondary antibodies were selected according to the host species of primary antibodies, and images were taken by using a digital imager (GE Healthcare Life Sciences, ImageQuant LAS 4000). The result was quantified using ImageJ.

Calculation of Normalized Tissue Labeling and Circulatory Turnover Flux—For those experiments where ^{13}C-isoleucine was infused along with unlabeled Valine and Leucine, normalized ^{13}C labeling of tissue metabolites represents the enrichment of tissue metabolite with ^{13}C label normalized to the steady-state tissue enrichment of isoleucine with m+6 isoleucine (Figure 4).

For those experiments where uniformly labeled ^{13}C-[Leu, Ile, Val] were infused in combination (Fig 2, 5), the contribution of BCAA-derived carbon to tissue metabolites represents the ^{13}C fractional enrichment of each metabolite normalized to the steady-state total BCAA plasma enrichment. The steady-state BCAA plasma enrichment was calculated as a weighted sum of BCAA plasma enrichment, where the enrichment of each BCAA was weighted according to its contribution to total BCAA R_d in each animal:

$$^{13}C\text{-}BCAA\ plasma\ enrichment = \frac{R_dIle}{R_dBCAA} * enrichment\ Ile + \frac{R_dVal}{R_dBCAA} * enrichment\ Val + \frac{R_dLeu}{R_dBCAA} * enrichment\ Leu$$

Whole-body carbon-atom circulatory turnover flux was calculated according to:

$$F_{atom\ circ} = R . \frac{1 - L}{L}$$

where R is the infusion rate of labeled tracer (nmol carbon/min/g) and L is the fractional carbon-atom labeling of the tracer.

Histologic Analysis—After completion of the study, hearts were removed, weighed, and a short axis slice was removed from mid-level ventricle. The slices were then laid into cassettes and fixed in 4% paraformaldehyde for further processing. Hearts were then paraffin-embedded, sliced with a microtome, and stained with haematoxylin/eosin and picrosirius blue for histological examination. Images were obtained with Keyence VHX-7000 microscope.

Dietary Conditions and BT2 Delivery—Apart from the BCKDH complex activity assay (Figure S3 K–M), all terminal experiments, isotopic infusions, and blood collections were performed at mid-day following a 5-hour fast. BCKDH activity was measured using tissue that was harvested in the morning from mice that had been permitted free access to food and water. All echocardiography was performed under ad-lib feeding conditions.

3,6-Dichlorobenzo[b]thiophene-2-carboxylic acid (BT2, Chem-Impex, Wood Dale, IL, Cat. 25643) was delivered via addition of BT2 to diet (250 mg/kg BT2 in AIN-76A diet, Research Diets Inc. New Brunswick, N.J.). BT2 content in chow was calculated to assuming 5 g food consumed per 27–30 g mouse/day (Bachmanov et al., 2002). BT2 and control AIN-76A diets were fully replaced at least every 3 days.

For comparison of BT2 plasma levels following BT2 diet vs. BT2 gavage, BT2 solution was given via gavage at 40 mg/kg. ~15–20 ul blood samples were taken via tail blood collection from ad-lib fed mice at 1, 6, and 24 hr post-gavage. Solution was prepared as described previously (Tso et al., 2014). BT2 was dissolved in DMSO and diluted into 5% DMSO, 10% cremophor EL, and 85% 0.1 M sodium bicarbonate, pH 9.0.

Telemetry—For telemetry experiments in Figure 7F and S7C, C57Bl6J mice (The Jackson Laboratory 664) bearing HD-X11 (Data Sciences International St. Paul, MN) radiotelemetry implants were received from Data Sciences International at 12 weeks of age and were given 1 week to acclimate to animal facility prior to data collection.

At the start of the telemetry data collection period, mice were individually housed in cages in a dedicated telemetry room with free access to food and water. The sequence of the experiment was as follows: all mice will be placed in cages and have a 3-day period where they were given standard facility chow (LabDiet 5010) and control water. Then to induce hypertension, all mice will be given control chow and L-NAME containing water for 3 days. On the night of day −1 (6PM), mice were moved to clean cages and switched from LabDiet 5010 to BT2-containing chow (250 mg/kg BT2 in AIN-76A, Research Diets Inc.) From days 0–6, mice received control water and BT2-containing chow, which was replaced every 2 days. On the evening of day 6, mice were moved to clean cages and given control AIN-76A diet (Research Diets Inc.). From the evening of day 6 (6PM)-evening of day 11 (6PM), mice received control water and control (AIN-76A) diet. From the evening of day 11 (6PM) -evening of day 14, mice received control (AIN-76A) diet and L-NAME (0.5 g/L, Sigma-Aldrich N5751) in drinking water with pH adjusted to 7.4 by addition of sodium

hydroxide. L-NAME water was made fresh and replaced every 2 days. From the evening of day 14 – end (day 23), mice received both BT2 diet and L-NAME in drinking water. Data were collected using Ponemah software (Data Sciences International, St. Paul, MN).

For telemetry experiment in Figure S7D and E, HD-X11 radiotelemetry implants were surgically implanted into the aortic arch (Mouse cardiovascular phenotyping core, University of Pennsylvania, PA) of C57BL6J mice (The Jackson Laboratory) or whole-body BCKDK−/− mice. Mice were allowed 1 week to recover. For Figure S7D, Mice were fed with each diet for 7 days in the order of control diet, 2xBCAA diet, control diet and 1/3 BCAA diet (Supplemental Table 5). Each diet was formulated based on control diet and corn starch was adjusted for calory match. For Figure S7E, mice were fed with control diet (AIN76A) for 7 days followed by BT2-containing diet for 7 days. Cage was changed every week along with diet. Out of seven days, last four days of stabilized data was averaged to plot.

Pressure myograph to measure vasodilatory function: Mice were fed either control AIN-76A diet or BT2 diet (250 mg BT2/kg AIN-76A diet, target dose 40 mg/kg/d) for 7 days prior to vasoreactivity study. Vasoreactivity was measured by using a DMT 114P pressure myography (DMT-USA). The mice were sacrificed by CO_2 asphyxiation, left carotid arteries were immediately removed, stripped of fat, and kept in HBSS in 37° C incubator until being secured to cannulas using silk sutures. Mounted vessels in the pressure myograph chamber were filled with warm HBSS containing either vehicle (DMSO) or BT2 in DMSO (80 uM BT2) and were visualized by light microscopy. The vessels were then pressurized gradually to 40, 60, and 100 mmHg. Arteries maintained at 100 mmHg were pre-constricted with phenylephrine (10^{-5} M) and then subjected to cumulative concentrations of acetylcholine (ACh; 10^{-9}M − 10^{-4}M) in the presence of phenylephrine to vasodilate. The vessel diameter change was continuously monitored using MYOVIEW II software (DMT-USA).

Mendelian Randomization—For the primary analysis, genetic variants associated with BCAA (isoleuceine, leucine, and valine) were identified from NMR metabolomics analysis from Kettunen et. al.(Kettunen et al., 2016). Inverse variance-weighted (or Wald-ratio MR if only 1 SNP available) MR was performed to test the association between circulating BCAA and SBP, DBP, MAP, and PP assessed among transancestry participants of UK Biobank. Multiple sensitivity analyses were performed. First, weighted-median and weighted-mode MR were performed, which make different assumptions about the presence of pleiotropy and invalid genetic instruments. In a second sensitivity analysis genetic instruments for BCAA were derived among ~115k participants of UKB. Associations between BCAA and BP traits were assessed using SBP and DBP GWAS from the previously reported ICBP+UKB meta-analysis (which included only individuals of European ancestry).

To test enrichment of independent (r^2 = 0.001, distance = 10,000kb, $p < 5\times10^{-8}$) BCAA-associated loci identified in either Kettunen, et. al., or the UK Biobank metabolite GWAS, SNPsnap (Pers et al., 2015) was used to identify 10,000 matched SNPs from across the genome for each lead BCAA-associated SNP based on allele frequency, number of SNPs in LD, distance to nearest gene, and gene density. The number of BCAA-associated variants located within 500kb of BCAA-pathway genes was compared to the null baseline

established across 10,000 permutations of matched SNPs to yield an empirical one-tailed p-value.

Quantification and Statistical Analysis—Data are presented as individual data points with means with error bars representing the standard error of the mean. T-test and repeated-measures ANOVA were used to calculate p values; the applicable test is reported in the legend accompanying each figure. Statistical analysis and graphs in Figures 1–6 and Supplemental Figures 1–6 was performed in GraphPad Prism (version 9.0). Mendelian Randomization was performed using R version 4.2.1. Experimental schematics were created using BioRender.

Supplementary Material

Refer to Web version on PubMed Central for supplementary material.

Acknowledgements

We thank the University of Pennsylvania CVI Mouse Phenotyping Core for surgeries and echocardiography. Telemetry and metabolomics were supported by the University of Pennsylvania DRC Rodent Metabolic Phenotyping Core and Metabolomics Core (NIH P30-DK19525 and S10-OD025098). Human heart tissue procurement was supported by R01 HL149891 and R01 HL105993. We thank the Gift-of-Life Donor Program, Philadelphia, PA, who helped provide nonfailing heart tissue. D.M. was supported by NHLBI (F30 HL142186-01A1) and the Blavatnik Family Foundation. M.D.N was supported by NIH 5T32CA257957. J.F.G. was supported by NIH (F32HL151146). M.G.L. was supported by the Institute for Translational Medicine and Therapeutics of the Perelman School of Medicine, the NIH/NHLBI (T32HL007843), and the Measey Foundation. E.F. was supported by NHLBI T32 HL 7954-20. M.H. was supported by Leducq (TNE FANTASY 19CV03). B.K. was supported by the ADA (1-18-PDF-153). E.R. and R.K.A. were supported by NIH AG162140. C.J. was supported by Edward Mallinckrodt Jr. Foundation. Z.A. was supported by NHLBI (HL152446), the Department of Defense (W81XWH18-1-0503), and Pfizer.

References

Abel ED, Kaulbach HC, Tian R, Hopkins JCA, Duffy J, Doetschman T, Minnemann T, Boers M-E, Hadro E, Oberste-Berghaus C, et al. (1999). Cardiac hypertrophy with preserved contractile function after selective deletion of GLUT4 from the heart. J Clin Invest 104, 1703–1714. 10.1172/jci7605. [PubMed: 10606624]

Bachmanov AA, Reed DR, Beauchamp GK, and Tordoff MG (2002). Food intake, water intake, and drinking spout side preference of 28 mouse strains. Behav Genet 32, 435–443. [PubMed: 12467341]

Bhattacharya S, Granger CB, Craig D, Haynes C, Bain J, Stevens RD, Hauser ER, Newgard CB, Kraus WE, Newby LK, et al. (2014). Validation of the association between a branched chain amino acid metabolite profile and extremes of coronary artery disease in patients referred for cardiac catheterization. Atherosclerosis 232, 191–196. 10.1016/j.atherosclerosis.2013.10.036. [PubMed: 24401236]

Chen M, Gao C, Yu J, Ren S, Wang M, Wynn RM, Chuang DT, Wang Y, and Sun H (2019). Therapeutic Effect of Targeting Branched- Chain Amino Acid Catabolic Flux in Pressure- Overload Induced Heart Failure. J Am Heart Assoc 8, e011625. 10.1161/jaha.118.011625. [PubMed: 31433721]

Clowes GHA, Randall HT, and Cha C-J (1980). Amino Acid and Energy Metabolism in Septic and Traumatized Patients. Jpen-Parenter Enter 4, 195–205. 10.1177/014860718000400225.

Du X, You H, Li Y, Wang Y, Hui P, Qiao B, Lu J, Zhang W, Zhou S, Zheng Y, et al. (2018a). Relationships between circulating branched chain amino acid concentrations and risk of adverse cardiovascular events in patients with STEMI treated with PCI. Sci Rep-Uk 8, 15809. 10.1038/s41598-018-34245-6.

Du X, Li Y, Wang Y, You H, Hui P, Zheng Y, and Du J (2018b). Increased branched-chain amino acid levels are associated with long-term adverse cardiovascular events in patients with STEMI and acute heart failure. Life Sci 209, 167–172. 10.1016/j.lfs.2018.08.011. [PubMed: 30092297]

Evangelou E, Warren HR, Mosen-Ansorena D, Mifsud B, Pazoki R, Gao H, Ntritsos G, Dimou N, Cabrera CP, Karaman I, et al. (2018). Genetic analysis of over 1 million people identifies 535 new loci associated with blood pressure traits. Nat Genet 50, 1412–1425. 10.1038/s41588-018-0205-x. [PubMed: 30224653]

Flam E, Jang C, Murashige D, Yang Y, Morley MP, Jung S, Kantner DS, Pepper H Jr., B. KC, Brandimarto J, et al. Integrated landscape of cardiac metabolism in end-stage human non-ischemic dilated cardiomyopathy. Nature Cardiovascular Research. In press.

Flores-Guerrero JL, Groothof D, Connelly MA, Otvos JD, Bakker SJL, and Dullaart RPF (2019). Concentration of Branched-Chain Amino Acids Is a Strong Risk Marker for Incident Hypertension. Hypertension 74, 1428–1435. 10.1161/hypertensionaha.119.13735. [PubMed: 31587574]

Förstermann U, Mülsch A, Böhme E, and Busse R (2018). Stimulation of soluble guanylate cyclase by an acetylcholine-induced endothelium-derived factor from rabbit and canine arteries. Circ Res 58, 531–538. 10.1161/01.res.58.4.531.

Hall GV, Saltin B, and Wagenmakers AJM (1999). Muscle protein degradation and amino acid metabolism during prolonged knee-extensor exercise in humans. Clin Sci 97, 557–567. 10.1042/cs0970557.

Hui S, Cowan AJ, Zeng X, Yang L, TeSlaa T, Li X, Bartman C, Zhang Z, Jang C, Wang L, et al. (2020). Quantitative Fluxomics of Circulating Metabolites. Cell Metab 32, 676–688.e4. 10.1016/j.cmet.2020.07.013. [PubMed: 32791100]

Ingwall JS, and Weiss RG (2004). Is the Failing Heart Energy Starved? Circ Res 95, 135–145. 10.1161/01.res.0000137170.41939.d9. [PubMed: 15271865]

Joshi MA, Jeoung NH, Obayashi M, Hattab EM, Brocken EG, Liechty EA, Kubek MJ, Vattem KM, Wek RC, and Harris RA (2006). Impaired growth and neurological abnormalities in branched-chain α-keto acid dehydrogenase kinase-deficient mice. Biochem J 400, 153–162. 10.1042/bj20060869. [PubMed: 16875466]

Kanai Y, Segawa H, Miyamoto K, Uchino H, Takeda E, and Endou H (1998). Expression Cloning and Characterization of a Transporter for Large Neutral Amino Acids Activated by the Heavy Chain of 4F2 Antigen (CD98)*. J Biol Chem 273, 23629–23632. 10.1074/jbc.273.37.23629. [PubMed: 9726963]

Kettunen J, Demirkan A, Würtz P, Draisma HHM, Haller T, Rawal R, Vaarhorst A, Kangas AJ, Lyytikäinen L-P, Pirinen M, et al. (2016). Genome-wide study for circulating metabolites identifies 62 loci and reveals novel systemic effects of LPA. Nat Commun 7, 11122. 10.1038/ncomms11122. [PubMed: 27005778]

Lahera V, Salom MG, Miranda-Guardiola F, Moncada S, and Romero JC (1991). Effects of NG-nitro-L-arginine methyl ester on renal function and blood pressure. Am J Physiol-Renal 261, F1033–F1037. 10.1152/ajprenal.1991.261.6.f1033.

Lai L, Leone TC, Keller MP, Martin OJ, Broman AT, Nigro J, Kapoor K, Koves TR, Stevens R, Ilkayeva OR, et al. (2014). Energy Metabolic Reprogramming in the Hypertrophied and Early Stage Failing Heart. Circulation Hear Fail 7, 1022–1031. 10.1161/circheartfailure.114.001469.

Li T, Zhang Z, Kolwicz SC, Abell L, Roe ND, Kim M, Zhou B, Cao Y, Ritterhoff J, Gu H, et al. (2017). Defective Branched-Chain Amino Acid Catabolism Disrupts Glucose Metabolism and Sensitizes the Heart to Ischemia-Reperfusion Injury. Cell Metab 25, 374–385. 10.1016/j.cmet.2016.11.005. [PubMed: 28178567]

Lu G, Sun H, She P, Youn J-Y, Warburton S, Ping P, Vondriska TM, Cai H, Lynch CJ, and Wang Y (2009). Protein phosphatase 2Cm is a critical regulator of branched-chain amino acid catabolism in mice and cultured cells. J Clin Invest 119, 1678–1687. 10.1172/jci38151. [PubMed: 19411760]

Mahbub MH, Yamaguchi N, Hase R, Takahashi H, Ishimaru Y, Watanabe R, Saito H, Shimokawa J, Yamamoto H, Kikuchi S, et al. (2020). Plasma Branched-Chain and Aromatic Amino Acids in Relation to Hypertension. Nutrients 12, 3791. 10.3390/nu12123791.

McCarthy JJ, Srikuea R, Kirby TJ, Peterson CA, and Esser KA (2012). Inducible Cre transgenic mouse strain for skeletal muscle-specific gene targeting. Skelet Muscle 2, 8. 10.1186/2044-5040-2-8. [PubMed: 22564549]

McGarrah RW, Crown SB, Zhang G-F, Shah SH, and Newgard CB (2018). Cardiovascular Metabolomics. Circ Res 122, 1238–1258. 10.1161/circresaha.117.311002. [PubMed: 29700070]

Melamud E, Vastag L, and Rabinowitz JD (2010). Metabolomic Analysis and Visualization Engine for LC–MS Data. Anal Chem 82, 9818–9826. 10.1021/ac1021166. [PubMed: 21049934]

Murashige D, Jang C, Neinast M, Edwards JJ, Cowan A, Hyman MC, Rabinowitz JD, Frankel DS, and Arany Z (2020). Comprehensive quantification of fuel use by the failing and nonfailing human heart. Science 370, 364–368. 10.1126/science.abc8861. [PubMed: 33060364]

Nakai N, Kobayashi R, Popov KM, Harris RA, and Shimomura Y (2000). [6] Determination of Branched-Chain α-Keto Acid Dehydrogenase Activity State and Branched-Chain α-Keto Acid Dehydrogenase Kinase Activity and Protein in Mammalian Tissues. Methods Enzymol 324, 48–62. 10.1016/s0076-6879(00)24218-3. [PubMed: 10989417]

Neinast MD, Jang C, Hui S, Murashige DS, Chu Q, Morscher RJ, Li X, Zhan L, White E, Anthony TG, et al. (2019). Quantitative Analysis of the Whole-Body Metabolic Fate of Branched-Chain Amino Acids. Cell Metab 29, 417–429.e4. 10.1016/j.cmet.2018.10.013. [PubMed: 30449684]

Neubauer S (2007). The Failing Heart — An Engine Out of Fuel. New Engl J Medicine 356, 1140–1151. 10.1056/nejmra063052.

Novarino G, El-Fishawy P, Kayserili H, Meguid NA, Scott EM, Schroth J, Silhavy JL, Kara M, Khalil RO, Ben-Omran T, et al. (2012). Mutations in BCKD-kinase Lead to a Potentially Treatable Form of Autism with Epilepsy. Science 338, 394–397. 10.1126/science.1224631. [PubMed: 22956686]

Pers TH, Timshel P, and Hirschhorn JN (2015). SNPsnap: a Web-based tool for identification and annotation of matched SNPs. Bioinformatics 31, 418–420. 10.1093/bioinformatics/btu655. [PubMed: 25316677]

Pisarenko OI, Solomatina ES, and Studneva IM (1986). The role of amino acid catabolism in the formation of the tricarboxylic acid cycle intermediates and ammonia in anoxic rat heart. Biochimica Et Biophysica Acta Bba - Mol Cell Res 885, 154–161. 10.1016/0167-4889(86)90083-2.

Pugach EK, Richmond PA, Azofeifa JG, Dowell RD, and Leinwand LA (2015). Prolonged Cre expression driven by the α-myosin heavy chain promoter can be cardiotoxic. J Mol Cell Cardiol 86, 54–61. 10.1016/j.yjmcc.2015.06.019. [PubMed: 26141530]

Rapoport RM, Draznin MB, and Murad F (1983). Endothelium-dependent relaxation in rat aorta may be mediated through cyclic GMP-dependent protein phosphorylation. Nature 306, 174–176. 10.1038/306174a0. [PubMed: 6316142]

Segawa H, Fukasawa Y, Miyamoto K, Takeda E, Endou H, and Kanai Y (1999). Identification and Functional Characterization of a Na+-independent Neutral Amino Acid Transporter with Broad Substrate Selectivity*. J Biol Chem 274, 19745–19751. 10.1074/jbc.274.28.19745. [PubMed: 10391916]

Shah SH, Bain JR, Muehlbauer MJ, Stevens RD, Crosslin DR, Haynes C, Dungan J, Newby LK, Hauser ER, Ginsburg GS, et al. (2010). Association of a Peripheral Blood Metabolic Profile With Coronary Artery Disease and Risk of Subsequent Cardiovascular Events. Circulation Cardiovasc Genetics 3, 207–214. 10.1161/circgenetics.109.852814.

Shah SH, Sun J-L, Stevens RD, Bain JR, Muehlbauer MJ, Pieper KS, Haynes C, Hauser ER, Kraus WE, Granger CB, et al. (2012). Baseline metabolomic profiles predict cardiovascular events in patients at risk for coronary artery disease. Am Heart J 163, 844–850.e1. 10.1016/j.ahj.2012.02.005. [PubMed: 22607863]

Sun H, Olson KC, Gao C, Prosdocimo DA, Zhou M, Wang Z, Jeyaraj D, Youn J-Y, Ren S, Liu Y, et al. (2016). Catabolic Defect of Branched-Chain Amino Acids Promotes Heart Failure. Circulation 133, 2038–2049. 10.1161/circulationaha.115.020226. [PubMed: 27059949]

Taegtmeyer H, Ferguson AG, and Lesch M (1977). Protein degradation and amino acid metabolism in autolyzing rabbit myocardium. Exp Mol Pathol 26, 52–62. 10.1016/0014-4800(77)90065-x. [PubMed: 832706]

Takala T, Hiltunen JK, and Hassinen IE (1980). The mechanism of ammonia production and the effect of mechanical work load on proteolysis and amino acid catabolism in isolated perfused rat heart. Biochem J 192, 285–295. 10.1042/bj1920285. [PubMed: 7305899]

Tso S-C, Gui W-J, Wu C-Y, Chuang JL, Qi X, Skvorak KJ, Dorko K, Wallace AL, Morlock LK, Lee BH, et al. (2014). Benzothiophene Carboxylate Derivatives as Novel Allosteric Inhibitors of Branched-chain α-Ketoacid Dehydrogenase Kinase*. J Biol Chem 289, 20583–20593. 10.1074/jbc.m114.569251. [PubMed: 24895126]

Uddin GM, Zhang L, Shah S, Fukushima A, Wagg CS, Gopal K, Batran RA, Pherwani S, Ho KL, Boisvenue J, et al. (2019). Impaired branched chain amino acid oxidation contributes to cardiac insulin resistance in heart failure. Cardiovasc Diabetol 18, 86. 10.1186/s12933-019-0892-3. [PubMed: 31277657]

Virani SS, Alonso A, Benjamin EJ, Bittencourt MS, Callaway CW, Carson AP, Chamberlain AM, Chang AR, Cheng S, Delling FN, et al. (2020). Heart Disease and Stroke Statistics—2020 Update. Circulation 141, e139–e596. 10.1161/cir.0000000000000757. [PubMed: 31992061]

Walejko JM, Christopher BA, Crown SB, Zhang G-F, Pickar-Oliver A, Yoneshiro T, Foster MW, Page S, van Vliet S, Ilkayeva O, et al. (2021). Branched-chain α-ketoacids are preferentially reaminated and activate protein synthesis in the heart. Nat Commun 12, 1680. 10.1038/s41467-021-21962-2. [PubMed: 33723250]

Wang W, Zhang F, Xia Y, Zhao S, Yan W, Wang H, Lee Y, Li C, Zhang L, Lian K, et al. (2016). Defective branched chain amino acid catabolism contributes to cardiac dysfunction and remodeling following myocardial infarction. Am J Physiol-Heart C 311, H1160–H1169. 10.1152/ajpheart.00114.2016.

Webb LA, Sadri H, von Soosten D, Dänicke S, Egert S, Stehle P, and Sauerwein H (2019). Changes in tissue abundance and activity of enzymes related to branched-chain amino acid catabolism in dairy cows during early lactation. J Dairy Sci 102, 3556–3568. 10.3168/jds.2018-14463. [PubMed: 30712942]

Yoneshiro T, Wang Q, Tajima K, Matsushita M, Maki H, Igarashi K, Dai Z, White PJ, McGarrah RW, Ilkayeva OR, et al. (2019). BCAA catabolism in brown fat controls energy homeostasis through SLC25A44. Nature 572, 614–619. 10.1038/s41586-019-1503-x. [PubMed: 31435015]

Highlights

- Systemic activation of BCAA oxidation lowers blood pressure and vascular resistance
- Enhanced whole-body BCAA oxidation is cardio-protective after myocardial infarction
- But cardiac-specific or muscle-specific activation of BCAA oxidation is not cardio-protective
- Improved vascular reactivity may explain cardio-protection by pro-BCAA oxidation agents.

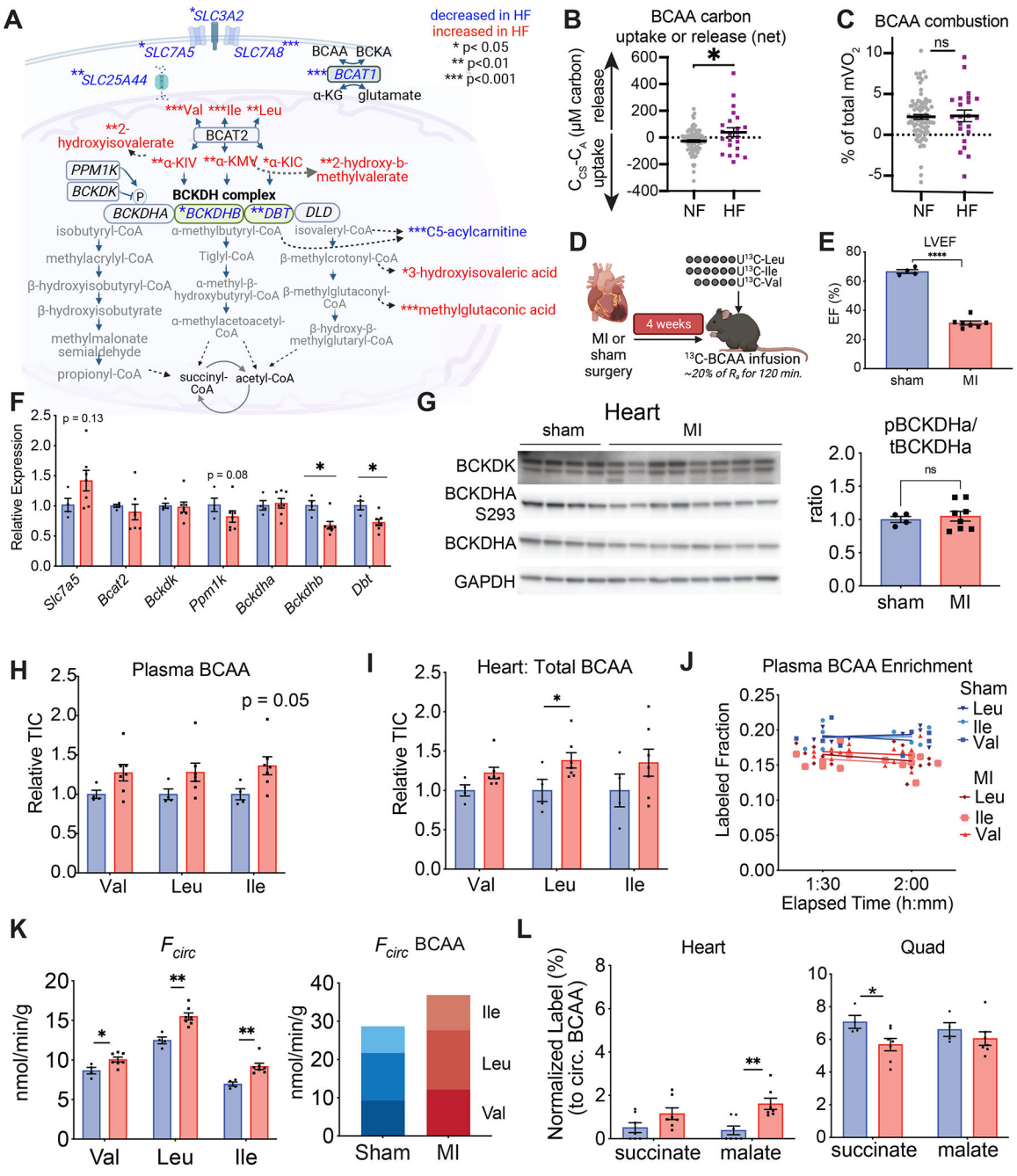

Figure 1: Alterations in the BCAA pathway in failing human myocardium, and increased preference for BCAA oxidation in murine heart failure.

(A) Schematic of BCAA uptake and oxidation pathway, and changes in gene expression or metabolite abundance in failing (HF) vs. non-failing (NF) human myocardium. Asterisks indicate nominal p value by student t-test.

(B) Total uptake or release of BCAA carbon by the failing (n = 23) or non-failing (n = 87) human heart. $C_{CS} - C_A$ = coronary sinus (CS) – artery (A).

(C) Contribution of BCAA carbon to myocardial oxygen consumption (mVO_2)

(D) Experimental scheme for (E)-(L).

(E) Cardiac function measured by echocardiography. LVEF: left ventricular ejection fraction. Sham: n = 4, MI: n = 7.

(F) Relative expression of indicated genes in left ventricle (LV) from sham or MI-treated animals. Error bars represent SEM. *p<0.05 by t-test.

(G) Western blot and quantification of pBCKDHA and total BCKDHA in LV from sham or MI-treated animals.

(H) Relative plasma levels of BCAAs in plasma following a 5-hr fast.

(I) Relative tissue levels of BCAAs in LV at the conclusion of infusion.

(J) Fractional labeling of plasma BCAAs with ^{13}C label during the final 30 minutes of infusion.

(K) Total circulatory flux (F_{circ}) of individual BCAAs (left) and total (right) BCAA carbon. *p<0.05, **p<0.01.

(L) Normalized labeling of TCA cycle intermediates in heart and quadriceps muscle at conclusion of infusion.

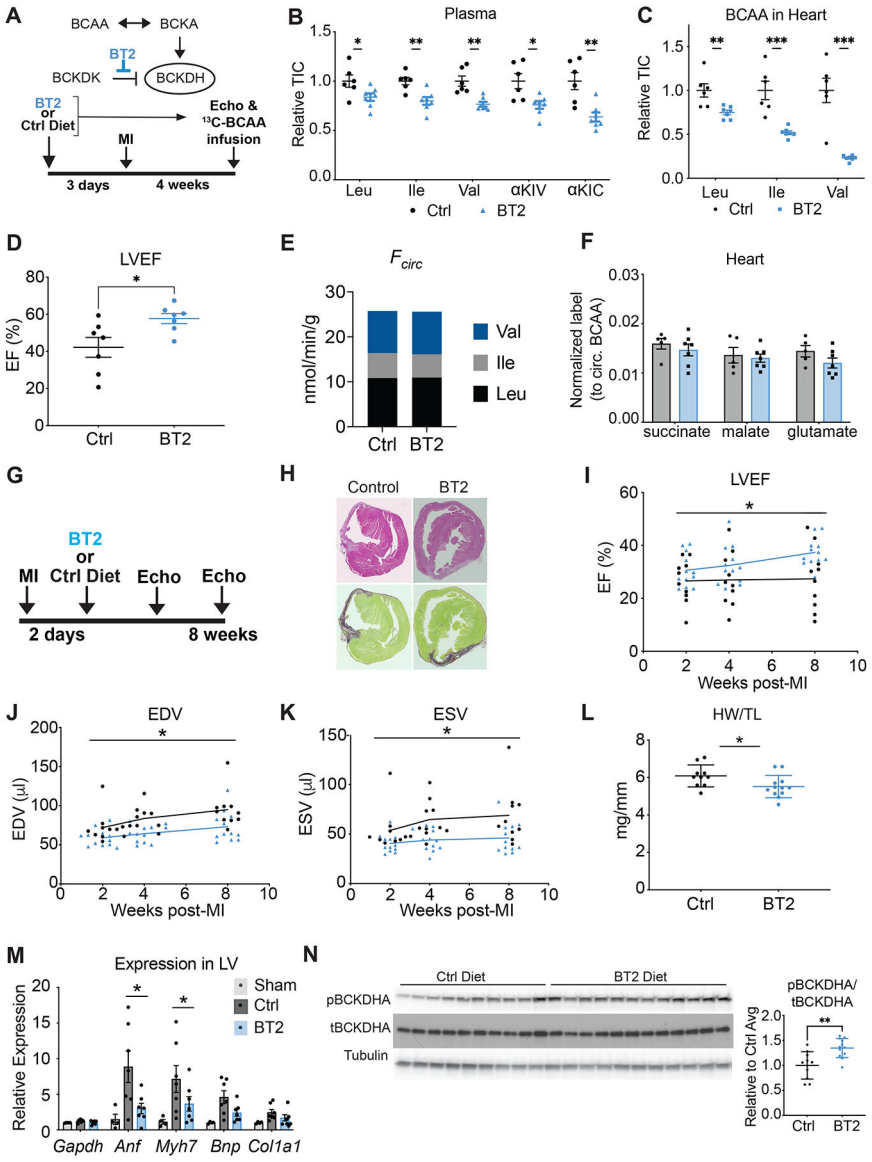

Figure 2: Global activation of BCAA catabolism improves cardiac remodeling pre-and post-myocardial infarction without affecting rates of cardiac BCAA oxidation.

(A) Experimental scheme for (B)-(F).

(B) Relative abundance of BCAA and BCKA in plasma 4 weeks post-MI in Ctrl or BT2-fed mice.

(C) Relative abundance of BCAA in heart 4 weeks post-MI.

(D) Left ventricular ejection fraction (LVEF), 4 weeks post-MI.

(E) Calculated total BCAA turnover flux (F_{circ}) of Leu, Ile, Val 4 weeks post-MI.

(F) Normalized cardiac ^{13}C labeling of TCA cycle intermediates and glutamate.

(G) Experimental scheme for (H)-(N).

(H) Representative H&E (top) and picrosirius blue (bottom) sections from myocardium 8 weeks post-MI.

(I-K) Left ventricular ejection fraction (LVEF), end-diastolic volume (EDV), and end-systolic volume (ESV) assessed up to 8 weeks post-MI. *p<0.05 by repeated-measures ANOVA.

(L) Heart weight/tibia length (HW/TL) ratio at 8 weeks post-MI.

(M) Relative expression of indicated genes. *p<0.05 by 1-way ANOVA

(N) Western blot and quantification of pBCKDHA S293 and total BCKDHa from heart.

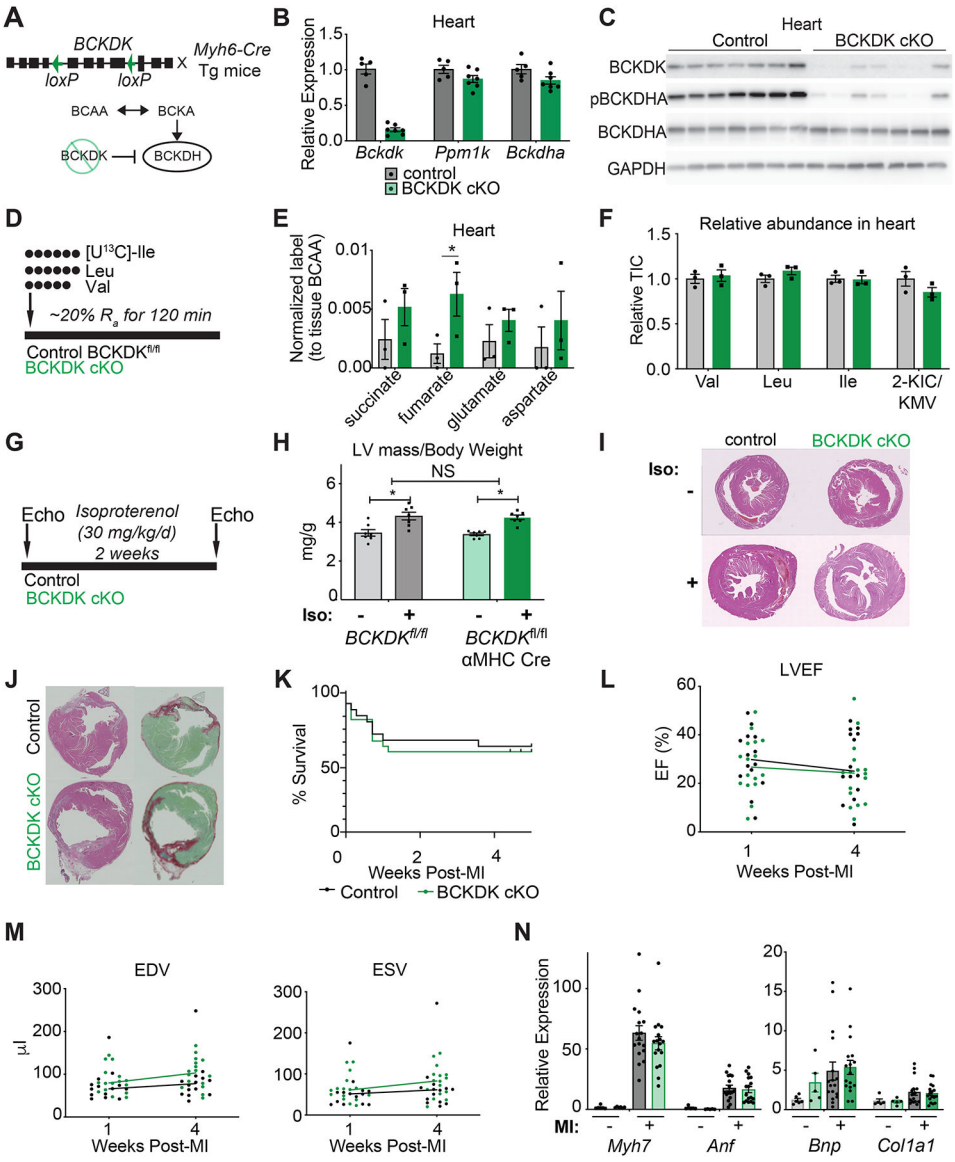

Figure 3: Activation of BCAA oxidation specifically in the heart does not confer cardiac benefit post-MI.

(A) Generation of cardiac-specific BCKDK KO (BCKDK cKO) mice.

(B) Relative expression of indicated genes in heart from control vs. BCKDK cKO mice.

(C) Immunoblot of BCKDK and BCKDK target pBCKDHA S293.

(D) Infusion scheme for (E)-(F).

(E) Normalized label of TCA cycle intermediates, glutamate, and aspartate in heart at conclusion of infusion.

(F) Relative abundance of BCAA in heart.

(G) Experimental scheme for (H)-(I).

(H) LV mass/Body Weight ratio at baseline vs. post-isoproterenol. *p<0.05 by 2-way ANOVA.

(I) Representative H&E sections from control vs. BCKDK cKO at baseline vs. post-isoproterenol treatment.

(J) Representative H&E (left) and picrosirius blue (right) sections from heart from control vs. BCKDK cKO 4 weeks post-MI.
(K) Survival post-MI of control vs. BCKDK cKO.
(L-M) Left ventricular ejection fraction (LVEF, **L**), end-diastolic, and end-systolic volume (EDV, ESV, **M)** from control vs. BCKDK cKO at 1 week and 4 weeks post-MI.
(N) Relative expression of indicated genes in LV from control vs. BCKDK cKO at 4 weeks post-MI.

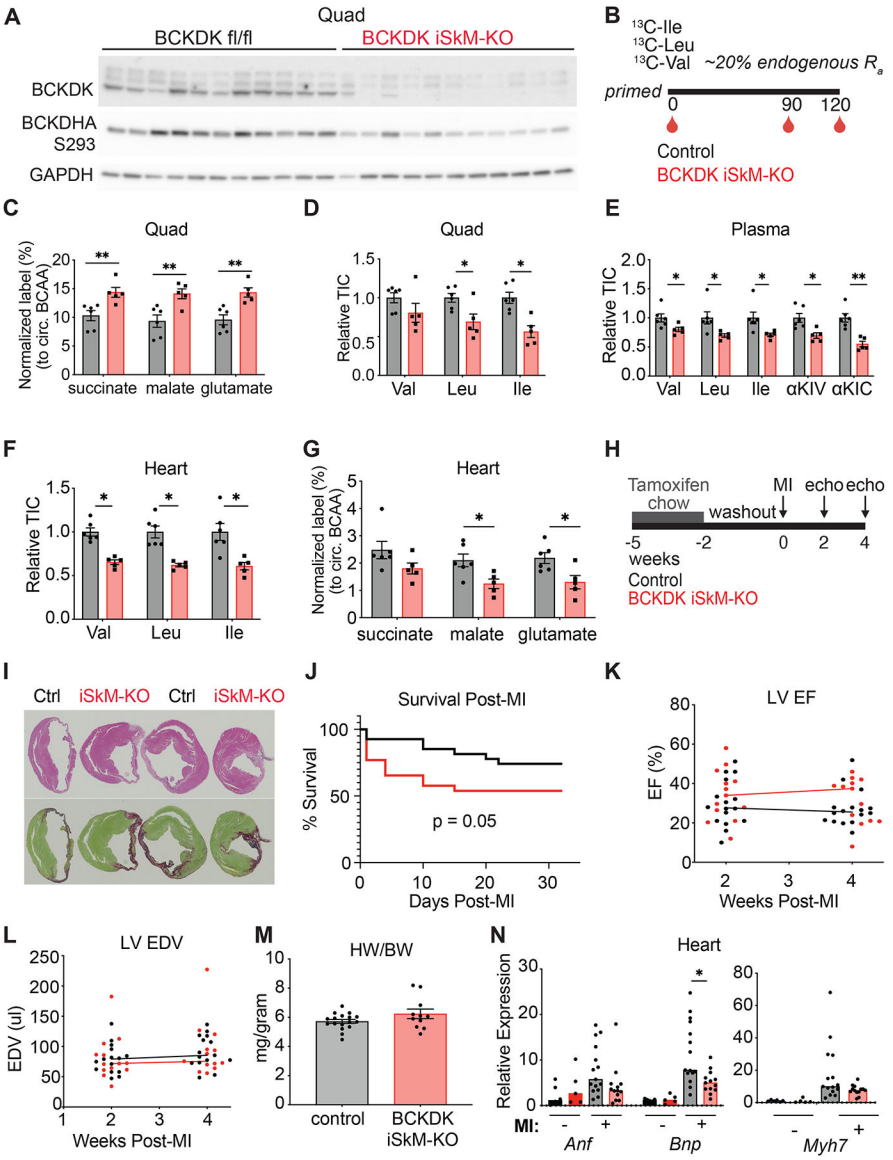

Figure 4: Activation of BCAA oxidation in skeletal muscle lowers plasma BCAA and confers mild cardiac benefit post-MI

(A) Western blot from quadriceps from control vs. skeletal muscle BCKDK KO (BCKDK iSkM-KO) mice.

(B) Infusion schematic.

(C) Fractional labeling of TCA intermediates and glutamate in quadriceps muscle.

(D-F) Relative abundance of BCAA in quadriceps muscle (D), plasma (E), and heart (F).

(G) Fractional labeling of TCA intermediates and glutamate in heart.

(H) Experimental scheme for (I)-(N).

(I) Representative H&E (top) and picrosirius blue (bottom) sections from heart post-MI.

(J) Survival post-MI analyzed by Gehan-Breslow-Wilcoxon test.

(K-L) Left ventricular ejection fraction (LVEF), left ventricular end-diastolic volume (EDV) at 2 and 4 weeks post-MI.

(M) Heart weight/body weight (HW/BW) at 4 weeks post-MI

(N) Relative expression of indicated genes in LV at baseline vs. post-MI. Hearts from infusion experiment were used for baseline comparison. * $p<0.05$ by t-test

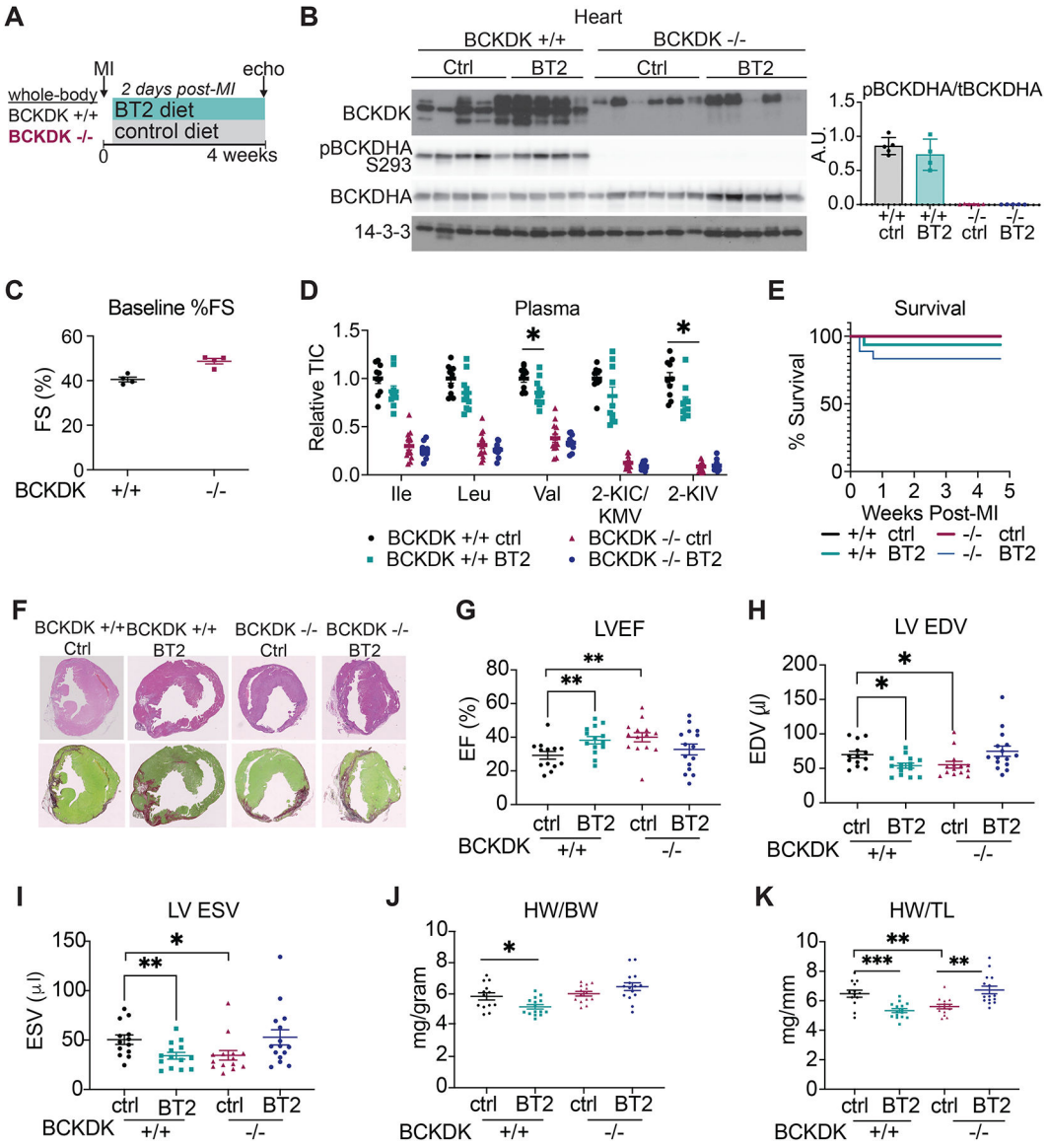

Figure 5: BT2 requires BCKDK to confer cardioprotection

(A) Experimental scheme.

(B) Western blot and quantification of indicated proteins from hearts at 4 weeks post-MI

(C) Baseline (pre-MI) left ventricular fractional shortening (%FS) assessed by echo

(D) Relative total ion counts (TIC) of BCAA and BCKA in plasma, 4 weeks post-MI

(E) Probability of survival following MI

(F) Representative H&E (top) and Picrosirius Blue stains from heart sections, 4 weeks post-MI

(G-I) Left ventricular EF (LVEF), end-diastolic (LVEDV), and end-systolic (LVESV) volume assessed at 4 weeks post-MI

(J-K) Heart weight to body weight (HW/BW) and to tibial length (HW/TL) post-MI

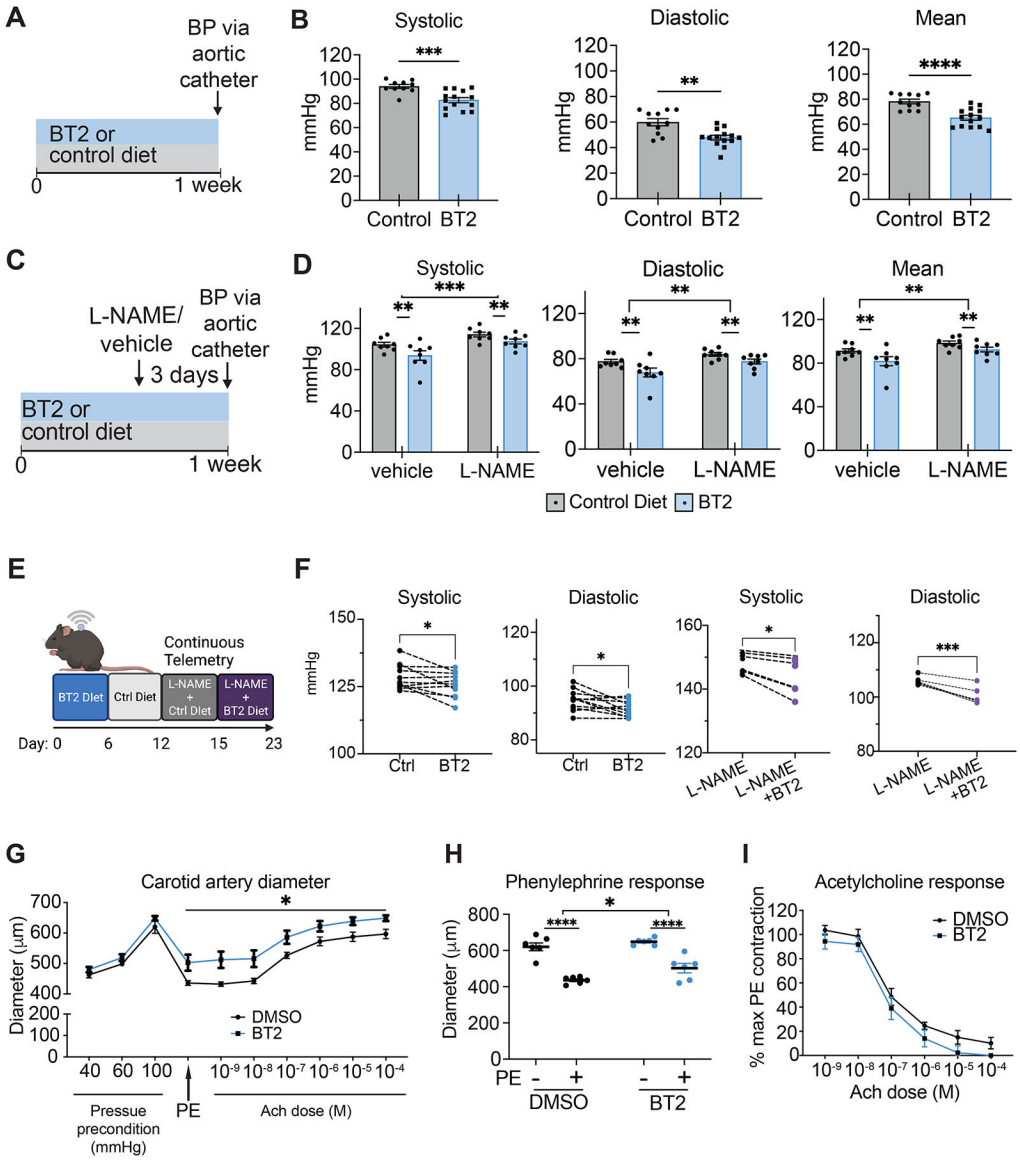

Figure 6: Global activation of BCAA catabolism promotes vasodilation and lowers blood pressure.

(A) Experimental scheme for (B). n=12/group.

(B) Systolic, diastolic, and mean BP averages measured via aortic catheter; 10 minutes recording/mouse. ** p< 0.01, ***<0.001, ****<0.0001 by t-test.

(C) Experimental scheme for (D). L-NAME: N^{ω}-nitro-L-arginine methyl ester (0.5 g/L in drinking water).

(D) Systolic, diastolic, and mean BP averages via aortic catheter; 10 minutes recording/ mouse. **p<0.01 by 2-way ANOVA.

(E) Experimental scheme for (F).

(F) BP recording from control vs. BT2 diet and L-NAME+control diet vs. L-NAME + BT2 diet conditions. Each dot represents average data of 1 mouse from indicated treatment period. Data are from dark cycle (8:00 PM – 6:00 AM). *p <0.05, ***p<0.001 by paired t-test.

(G) Diameter of carotid artery from mice treated with 7 days control diet + DMSO in buffer (n = 6) or 7 days BT2 diet + BT2 in buffer (n = 6). Following pressure pre-condition, phenylephrine (10^{-5} M) was added, followed by indicated amounts of acetylcholine. * $p<0.05$ by repeated measures ANOVA.
(H-I) Response to phenylephrine (H) and acetylcholine (I) in DMSO vs. BT2 condition. *$p<0.05$, 2-way ANOVA

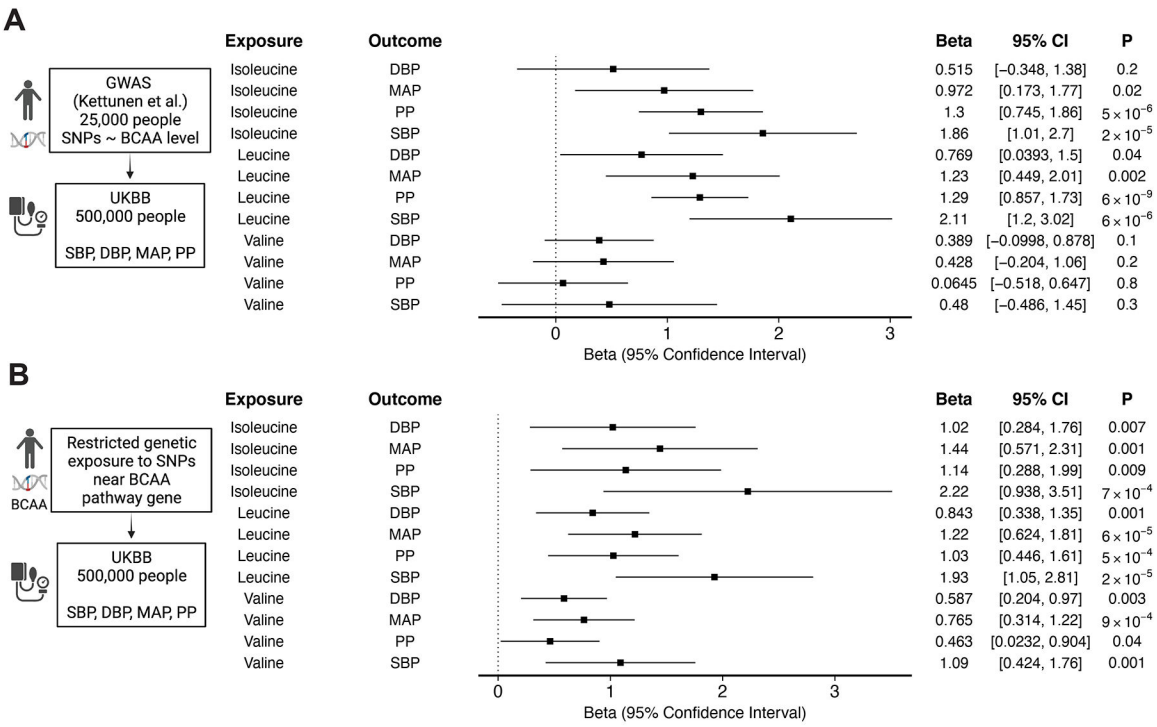

Figure 7: Mendelian Randomization studies support a causal relationship between BCAAs and blood pressure in human cohorts

(A) In inverse variance-weighted Mendelian randomization (MR) analyses, elevations in leucine predicted higher systolic, mean, and pulse pressure; elevations in isoleucine predicted higher systolic and pulse pressure.

(B) Secondary MR restricted to SNPs within 500kb of one of 14 genes unique to BCAA catabolic pathway.

KEY RESOURCES TABLE

REAGENT or RESOURCE	SOURCE	IDENTIFIER
Antibodies		
Anti-total BCKDK	Abcam	Cat#: ab128935
Anti-phospho-BCKDHA Ser293	Bethyl	Cat#: A304–672A
Anti-total BCKDHA	Bethyl	Cat#: Bethyl A303–790A
Anti-ß-Tubulin	Cell Signaling	Cat#: 2128
Anti-GAPDH	Cell Signaling	Cat#: 2118
Anti-14-3-3	Cell Signaling	Cat#: 9636
Anti-total DBT	Proteintech	Cat#: 12451–1-AP
Anti-phospho ULK1 S757	Cell Signaling Technology	Cat#: 6888
Anti-total ULK1	Cell Signaling Technology	Cat#: 8054
Anti-phospho S6K Thr389	Cell Signaling Technology	Cat#: 9234
Anti-p4e-BP1 Thr37/46	Cell Signaling Technology	Cat#: 2855
Anti-total 4e-BP1	Cell Signaling Technology	Cat#: 9644
Anti-pS6 Ser235/236	Cell Signaling Technology	Cat#: 4858
Anti-BCKDHB	Sigma-Aldrich	Cat#: HPA031580
Anti-BCAT2	Cell Signaling Technology	Cat#: 9432S
Chemicals, Peptides, and Recombinant Proteins		
TRIzol	ThermoFisher	Cat#: 15596026
Isoproterenol	Sigma-Aldrich	Cat#: I6504
2,2,2-Tribromoethanol	Sigma-Aldrich	Cat#: T48402
L-LEUCINE (13C6, 99%)	Cambridge Isotope Laboratories, Inc.	Cat#: CLM-2262-H-PK
L-ISOLEUCINE (13C6, 99%)	Cambridge Isotope Laboratories, Inc.	Cat#: CLM-2248-H-PK
L-VALINE (13C5, 99%)	Cambridge Isotope Laboratories, Inc.	Cat#: CLM-2249-H
PhosSTOP phosphatase inhibitor	Roche	Cat#: 4906845001
Complete miniproteinase inhibitor	Roche	Cat#: 5892970001
3,6-Dichlorobenzo[β]thiophene-2-carboxylic acid	Chem-Impex	Cat#: 25643
Critical Commercial Assays		
High-Capacity cDNA Reverse Transcription Kit	ThermoFisher	Cat#: 4368813
Ultra sensitive mouse insulin ELISA	Crystal Chem	Cat#: 90080
Deposited Data		
RNAseq: Control vs. non-ischemic dilated cardiomyopathy human myocardium (Figure 1)	This study	GSE14190
Metabolomics (human plasma): Control vs. non-ischemic dilated cardiomyopathy, related to Figure 1	This study	MTBLS5734
Metabolomics (human myocardium): Control vs. non-ischemic dilated cardiomyopathy, related to Figure 1	This study	MTBLS5734
Experimental Models: Organisms/Strains		
Mouse: *αMHC-Cre:* Tg(Myhca-cre)1Abel	Abel et al., 1999	MGI:2182091
Mouse: *HSA-Cre:* Tg(ACTA1-cre/Esr1*)2Kesr/J	The Jackson Laboratory	Cat#: 025750

REAGENT or RESOURCE	SOURCE	IDENTIFIER
Mouse: *Cmv-Cre* : B6.C-Tg(CMV-cre)1Cgn/J	The Jackson Laboratory	Cat#: 006054
Mouse: *Bckdk*$^{fl/fl}$	This study	N/A
Oligonucleotides		
Oligonucleotides	See Table S6	N/A
Software and Algorithms		
MAVEN Software	Melamud et al.	http://genomics-pubs.princeton.edu/mzroll/index.php
GraphPad Prism 9	GraphPad Software	https://www.graphpad.com
Mendelian randomization analysis	This study	https://doi.org/10.5281/zenodo.7012972
Other		
Subcutaneous osmotic pump	DURECT corporation	Cat#: Alzet 1002
Microvette® CB 300 Lithium heparin, capillary blood collection	Sarstedt	Cat#: 16.443.100
XBridge BEH Amide XP column	Waters	Cat#: 176002889
Normal Chow Diet	LabDiet	Cat#: 5001
BT2 Diet and matching control	See Table S5	N/A
High-BCAA, Low-BCAA, and Control-BCAA Diet	See Table S6	N/A